Cell Reports

Article

# Temporal analysis suggests a reciprocal relationship between 3D chromatin structure and transcription

## Graphical abstract

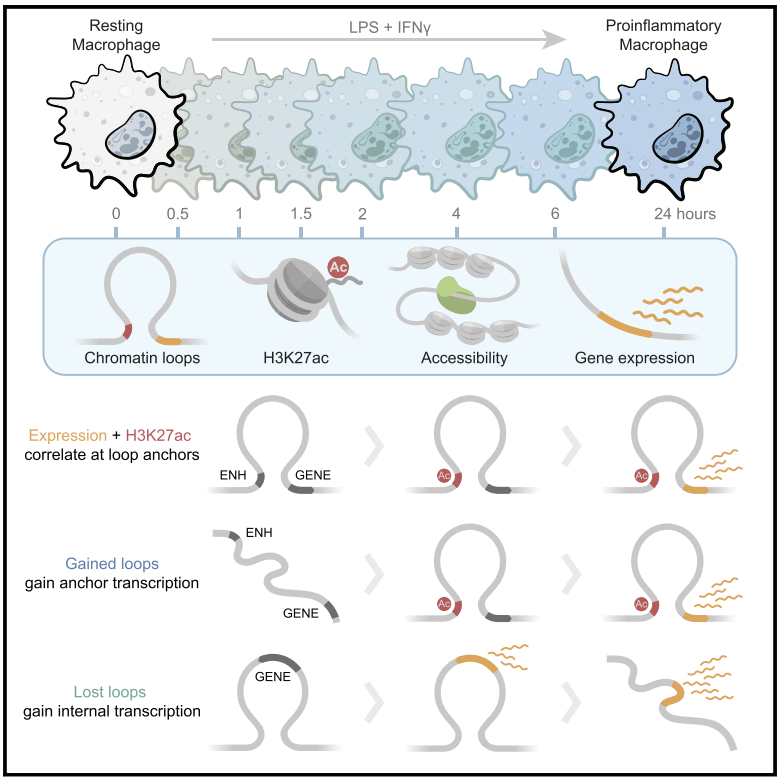


## Authors

Kathleen S.M. Reed, Eric S. Davis, Marielle L. Bond, ..., Hyejung Won, Michael I. Love, Douglas H. Phanstiel

## Correspondence

douglas_phanstiel@med.unc.edu

## In brief

Chromatin loops connect genes and distal regulatory elements, but their function remains unclear. Reed et al. compare genome-wide changes in chromatin looping, gene expression, and enhancer acetylation over time as macrophages respond to stimulus. They find evidence that chromatin structure supports and is shaped by transcriptional changes.

## Highlights

- LPS + IFN$_\gamma$ treatment triggers genome-wide changes in chromatin loops, acetylation, expression
- Looped enhancer-promoter pairs show ordered changes in acetylation and expression
- Changes in gene expression exhibit a directional bias at differential loop anchors
- Lost loops are associated with high levels of transcription within loop boundaries

Reed et al., 2022, Cell Reports *41*, 111567
November 1, 2022 
https://doi.org/10.1016/j.celrep.2022.111567

CellPress

Cell Reports

CellPress
OPEN ACCESS

Article

# Temporal analysis suggests a reciprocal relationship between 3D chromatin structure and transcription

Kathleen S.M. Reed,[1,11] Eric S. Davis,[2,11] Marielle L. Bond,[1] Alan Cabrera,[3] Eliza Thulson,[1] Ivana Yoseli Quiroga,[4] Shannon Cassel,[4] Kamisha T. Woolery,[4] Isaac Hilton,[3,5] Hyejung Won,[6,7] Michael I. Love,[8,9] and Douglas H. Phanstiel[1,2,4,10,12,*]

[1]Curriculum in Genetics and Molecular Biology, University of North Carolina, Chapel Hill, NC 27599, USA
[2]Curriculum in Bioinformatics and Computational Biology, University of North Carolina, Chapel Hill, NC 27599, USA
[3]Department of Bioengineering, Rice University, Houston, TX 77005, USA
[4]Thurston Arthritis Research Center, University of North Carolina, Chapel Hill, NC 27599, USA
[5]Department of Biosciences, Rice University, Houston, TX 77005, USA
[6]Department of Genetics and Neuroscience Center, University of North Carolina, Chapel Hill, NC 27599, USA
[7]Neuroscience Center, University of North Carolina, Chapel Hill, NC 27599, USA
[8]Department of Genetics, University of North Carolina, Chapel Hill, NC 27599, USA
[9]Department of Biostatistics, University of North Carolina, Chapel Hill, Chapel Hill, NC 27599, USA
[10]Department of Cell Biology and Physiology, University of North Carolina, Chapel Hill, NC 27599, USA
[11]These authors contributed equally
[12]Lead contact
*Correspondence: douglas_phanstiel@med.unc.edu
https://doi.org/10.1016/j.celrep.2022.111567

## SUMMARY

To infer potential causal relationships between 3D chromatin structure, enhancers, and gene transcription, we mapped each feature in a genome-wide fashion across eight narrowly spaced time points of macrophage activation. Enhancers and genes connected by loops exhibit stronger correlations between histone H3K27 acetylation and expression than can be explained by genomic distance or physical proximity alone. At these looped enhancer-promoter pairs, changes in acetylation at distal enhancers precede changes in gene expression. Changes in gene expression exhibit a directional bias at differential loop anchors; gained loops are associated with increased expression of genes oriented away from the center of the loop, and lost loops are often accompanied by high levels of transcription within the loop boundaries themselves. These results are consistent with a reciprocal relationship where loops can facilitate increased transcription by connecting promoters to distal enhancers, whereas high levels of transcription can impede loop formation.

## INTRODUCTION

3D chromatin structure is thought to play a critical role in gene expression, cellular identity, and organismal development by modulating contact frequencies between gene promoters and distal regulatory elements such as enhancers (Dekker and Mirny, 2016). Alterations in 3D chromatin architecture have been associated with developmental abnormalities and human disease (Spielmann et al., 2018; Akdemir et al., 2020; Johnstone et al., 2020; Rosencrance et al., 2020; Ahn et al., 2021). Despite growing knowledge regarding the proteins and molecules that govern 3D chromatin architecture, the relationship between 3D chromatin architecture and gene transcription is less certain. Although some functional connections between chromatin interactions and transcription have been established, the degree to which 3D chromatin structure shapes—or is shaped by—transcription remains unclear.

The continued development of chromatin conformation capture (3C)-based technologies has provided valuable insights into the mechanisms driving 3D chromatin structure (Dekker et al., 2002; Dostie et al., 2006; Simonis et al., 2006; Fullwood et al., 2009; Lieberman-Aiden et al., 2009; Rao et al., 2014; Mumbach et al., 2016). In particular, genome-wide approaches, including Hi-C, have revealed tens of thousands of loops throughout the human genome, many of which connect regulatory elements such as enhancers to gene promoters. With some notable exceptions (Lee et al., 2017; Monahan et al., 2019; Ahn et al., 2021), the majority of loops are bound at each anchor by CCCTC-binding factor (CTCF) and are formed via loop extrusion by the cohesin complex (Heidari et al., 2014; Sanborn et al., 2015). Mapping these loops across cell types and biological conditions has revealed cell-type-specific looping events that often correlate with differences in gene transcription (Rao et al., 2014; Phanstiel et al., 2017; D'Ippolito et al., 2018; Winick-Ng et al., 2021).

Despite these advances, the mechanisms and degree to which looping drives transcriptional changes are far less certain.

A widely held hypothesis is that chromatin loops facilitate transcriptional activation by increasing the frequency of interactions between enhancers and gene promoters; however, studies that removed looping genome wide have produced conflicting results. Acute depletion of cohesin in a human cancer cell line was sufficient to eliminate cohesin-bound loops but had only a modest effect on transcription, casting doubt on the importance of DNA looping for transcriptional control (Rao et al., 2017). In contrast, deletion of the cohesin loading factor NIPBL (Nipped B-like protein) in mouse liver cells *in vivo* induced transcriptional changes of thousands of genes (Schwarzer et al., 2017). Depletion of cohesin and CTCF has been shown to significantly affect the ability of human and mouse macrophages to mount a proper transcriptional response to the endotoxin lipopolysaccharide (LPS) (Cuartero et al., 2018; Stik et al., 2020), which suggests that loops might be specifically important for regulating changes to (as opposed to maintenance of) transcriptional signatures.

Mounting evidence also suggests that transcription can shape 3D chromatin structure, although the exact relationship remains unclear. Several studies have shown that transcription can displace cohesin and condensin complexes (Lengronne et al., 2004; Busslinger et al., 2017; Brandão et al., 2019). For example, knocking down CTCF and the cohesin unloader WAPL (Wings apart-like protein homolog) causes cohesin to accumulate at the 3′ end of highly transcribed genes, suggesting that cohesin may be relocated by transcription in the absence of boundary elements (Busslinger et al., 2017). Other work has demonstrated that transcription-induced displacement of structural maintenance of chromsosome (SMC) complexes results in altered chromatin structure. Macrophages infected with influenza A, which inhibits transcription termination, show readthrough transcription that displaces cohesin at CTCF binding sites, repositioning it toward the 3′ end of genes and disrupting existing chromatin structure (Heinz et al., 2018). Fibroblasts undergoing senescence exhibit *de novo* transcription-dependent cohesin peaks at the 3′ end of select genes, resulting in newly formed loops (Olan et al., 2020). Alternatively, knockdown of RNA polymerase II (-RNAPII) causes new loops to form at CTCF anchors and many enhancer-promoter loops to be lost (Zhang et al., 2022). These findings are supported by *in vitro* experiments performed on DNA "curtains," showing that RNAP or other translocases can push cohesin; however, more recent studies suggest that molecules as large as 200 nm may be able to pass through SMC complexes (Davidson et al., 2016; Stigler et al., 2016; Pradhan et al., 2021).

One approach to dissect causal relationships between looping and transcription while circumventing genome-wide perturbations with potential knock-on effects is to quantify changes in looping, transcription, and other regulatory features across biological time courses. 3C-based time courses of biological transitions have produced valuable insights into the dynamics of 3D chromatin architecture (Bonev et al., 2017; Abramo et al., 2019; Bertero et al., 2019; Zhang et al., 2019a, 2019b; Yang et al., 2020; Furlan-Magaril et al., 2021; Vilarrasa-Blasi et al., 2021). For example, D'Ippolito et al. (2018) characterized differential looping at 4 time points after glucocorticoid treatment and found that, on average, loops changed maximally at 4 h, whereas gene expression changed maximally at 9 h. This timing is consistent with a regulatory relationship, but the relatively broad spacing of time points made temporal ordering of individual pairs of loops and genes more difficult. Beagan et al. (2020) used chromosome conformation capture carbon copy (5C) to identify differential looping events in activated neurons in time frames as short as 20 min (Beagan et al., 2020); however, these studies focused on just a handful of genomic loci.

To characterize the temporal order of regulatory events and infer potential causal relationships, we mapped 3D chromatin architecture, histone H3K27 acetylation, chromatin accessibility, and gene expression across eight time points of macrophage activation. Narrowly spaced timepoints allowed correlation and temporal ordering of events at a locus-by-locus level. These analyses provided insights into the putative causal relationships between these events, which were consistent with a reciprocal relationship between chromatin looping and gene transcription.

## RESULTS

### LPS + IFN$_\gamma$ treatment triggers genome-wide changes in chromatin looping, enhancer acetylation, and gene expression

To understand how chromatin loops and enhancers work together to regulate gene transcription in response to external stimuli, we used an eight-point time course of human macrophage activation (Figure 1A). Human macrophages derived from the THP-1 monocytic cell line were stimulated with 10 ng/mL LPS and 20 ng/mL interferon-gamma (IFN$_\gamma$) and collected at eight time points (0, 0.5, 1, 1.5, 2, 4, 6, and 24 h). At each time point, we profiled 3D chromatin structure using *in situ* Hi-C (Rao et al., 2014), putative enhancer activity using chromatin immunoprecipitation sequencing (ChIP-seq) targeting histone 3 lysine 27 acetylation (H3K27ac), chromatin accessibility using assay for transposase-accessible chromatin using sequencing (ATAC-seq; Buenrostro et al., 2013), and gene expression using RNA sequencing (RNA-seq).

With eight time points and roughly 2 billion contacts per Hi-C map, this is one of the most comprehensive characterizations of 3D chromatin changes to date (D'Ippolito et al., 2018; Rowley et al., 2020). To comprehensively catalog long-distance chromatin interactions, we combined our maps from each time point into a single, ultra-deep "mega" map comprising 24.5 billion reads and 15.6 billion chromatin contacts (Figures S1A and S1B). This increased read depth provided the power to identify over 10,000 additional loops at 5-kb resolution that were undetectable at the resolution of individual time points (Figure S1C). Loops from each timepoint as well as the Mega map were then merged, combining any loops with both anchors within 20 kb to provide 42,690 total loops for this study.

To identify potential regulatory connections among these loops, we classified putative enhancers (hereafter called enhancers) as loci with overlapping ATAC-seq and histone H3K27 acetylation peaks that did not overlap gene promoters (STAR Methods). Intersecting these enhancers with chromatin loops revealed 5,039 enhancer-promoter loops (Figure 1B). The regulatory activity of enhancers was inferred via quantification of histone H3K27ac at each enhancer. Finally, we used stranded rRNA-depleted RNA-seq at each time point to quantify

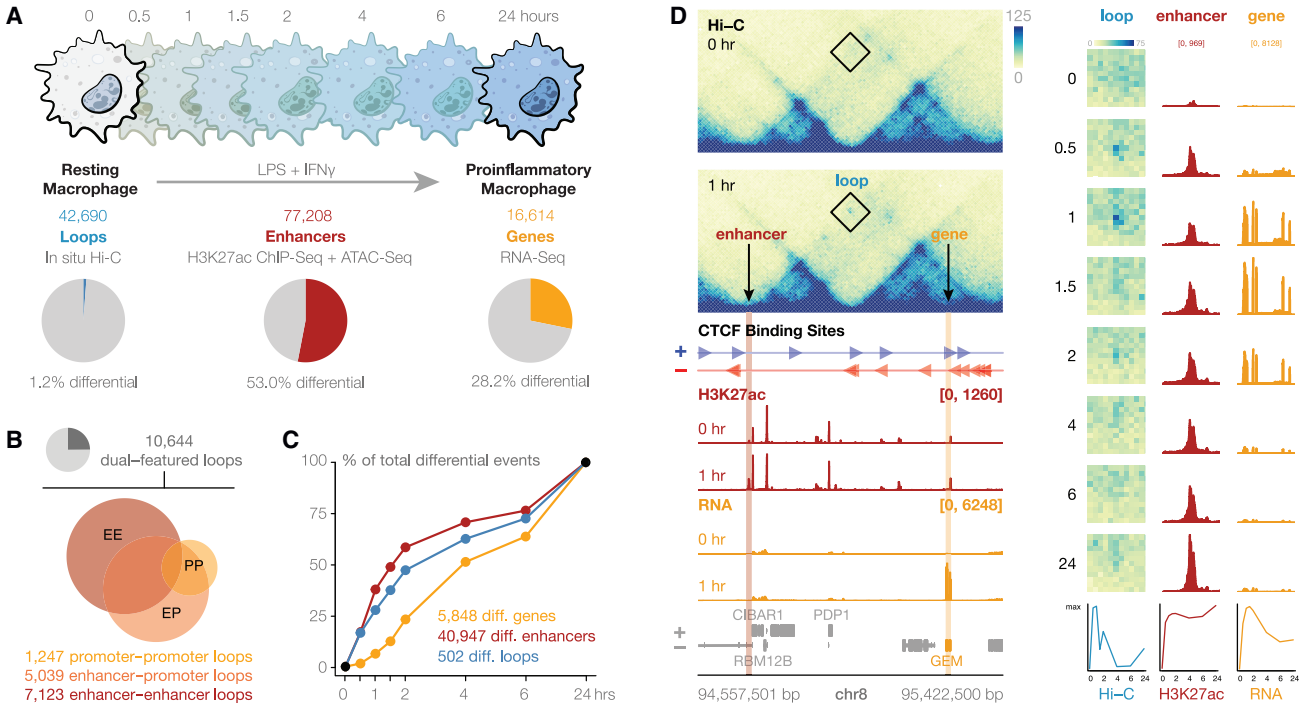


**Figure 1. Multi-omics time course of macrophage activation physically and temporally connects regulatory events**

(A) Experimental design to identify changes to 3D chromatin structure, enhancers, and gene expression across eight time points during macrophage proinflammatory activation. Differential chromatin loops were identified using Hi-C from 5 technical replicates across 3 biological replicates for a total of roughly 2 billion contacts per time point. Differential H3K27ac peaks and genes were identified from 2 biological replicates of H3K27ac ChIP-seq and RNA-seq, respectively.

(B) Fraction and number of loops that connect two distal elements.

(C) A cumulative sum of differential events identified by each time point reveals the relative timing of changes to genes, loops, and enhancers.

(D) Intersecting differential chromatin loops, enhancers, and genes provides the regulatory context of transcriptional changes. Predicted CTCF binding sites obtained from the *CTCF* R package are also shown for this locus. At this region, a 570-kb loop connects the promoter of the *GEM* gene to a distal enhancer. The enhancer's activity peaks 30 min before gene expression but remains high throughout the treatment, whereas the loop connecting them fades alongside gene expression after 2 h. Line plots show the log2 fold change of Hi-C, enhancer H3K27ac, and *GEM* expression signal over the full time course. Hi-C is shown at 10-kb resolution for the full region and 5-kb resolution for the loop magnifications. Scales indicate read signal (RNA, ChIP) or KR-normalized counts (Hi-C).

the potential effects of these loops and enhancers on gene expression.

Differential analysis using the DESeq2 package (Love et al., 2014) identified statistically significant genome-wide alterations in DNA looping, enhancer activity, and gene expression at each time point (Figures 1C, S2A, Tables S1, S2, and S3). The transcriptional changes we observed are consistent with previously established profiles of inflammatory activation (Figures S2B ad S2C). Only 1.2% (220 up, 282 down) of loops were detected as differential for at least one time point compared with 53.0% (21,858 up, 19,089 down) of enhancers and 28.2% (3,025 up, 2,823 down) of genes. Of these 502 differential loops, 79 were detected only at intermediate time points and were not visible at 0 or 24 h, highlighting the insights offered from this level of temporal resolution. On average, enhancers and loops changed faster than genes, with 58.4% of differential enhancers and 47.2% of differential loops changing significantly within the first 2 h of LPS + IFN$_\gamma$ treatment compared with only 23.1% of genes (Figure 1C). This temporal lag between changes in loops and enhancers compared with changes in gene expression is consistent with our understanding of loops and enhancers as regulators of gene transcription and highlights the power of using temporal analysis to generate hypotheses about causal relationships (Arner et al., 2015; Rowley and Corces, 2018; Schoenfelder and Fraser, 2019; Zheng and Xie, 2019).

Integrating the resulting multi-omics data provided insights into gene-regulatory mechanisms of macrophage activation. An example of this concept can be seen at the *GEM* locus on chromosome 8 (Figures 1D, S2D, and S2E). The *GEM* gene is transiently upregulated during LPS + IFN$_\gamma$ treatment, with expression increasing at 30 min and peaking at 1.5 h. An enhancer 570 kb downstream of the *GEM* promoter becomes acetylated and physically looped to the promoter of *GEM* after only 30 min of treatment, coinciding with increased expression of GEM. Although the enhancer remains acetylated throughout the time course, a precipitous drop in contact frequency between the enhancer and promoter at 1.5 h is followed by a similar decrease in gene expression 30–60 min later. These data are consistent with a model in which contacts between active enhancers and gene promoters play a causal role in transcriptional changes. Throughout the rest of this paper, we explore these relationships quantitatively on a genome-wide scale.

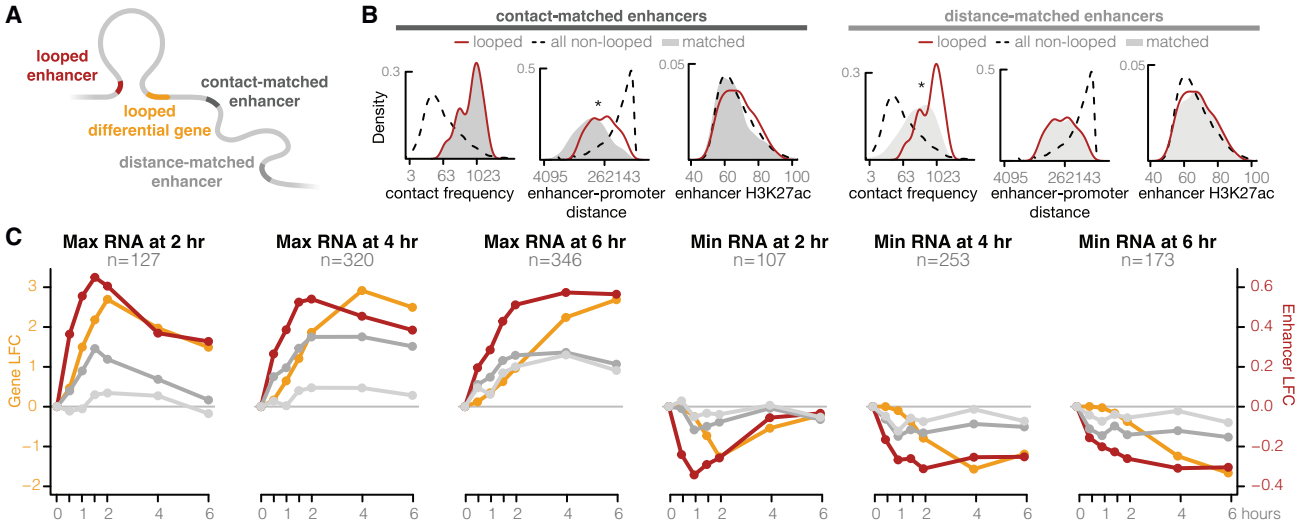


**Figure 2. Enhancer acetylation and gene expression correlate most highly at looped enhancer-promoter pairs**

(A) Distal enhancers looped to the promoters of differential genes were compared with matched enhancers of equal H3K27ac and contact frequency (dark gray) or distance (light gray).

(B) Representative distributions of contact- and distance-matched enhancers compared with the pool of non-looped enhancer-promoter pairs and the looped subset. Compared with looped pairs, contact-matched enhancers are closer on average in base pairs (Wilcoxon rank-sum test, $p < 10^{-6}$), whereas distance-matched enhancers are in less frequent contact (Wilcoxon rank-sum test, $p < 10^{-11}$). Both sets of matched enhancers have H3K27ac levels similar to the looped pairs (Wilcoxon rank-sum test, $p = 0.028, 0.86$).

(C) Average log2 fold change of gene expression (gold) for genes reaching minimum or maximum fold change at 2, 4, or 6 h compared with log2 fold change of the H3K27ac levels of their looped enhancers (red), contact-matched enhancers (dark gray), and distance-matched enhancers (light gray). Looped enhancers correlate significantly with changes in gene expression, to a larger extent than matched enhancers. Contact-matched enhancers tend to correlate better than distance-matched enhancers at upregulated genes. Changes in distal enhancer H3K27 acetylation precede changes in gene expression among all time scales and among up- and downregulated genes.

## Looped enhancer-promoter pairs exhibit ordered and correlated changes in acetylation and expression

The importance of chromatin looping for transcriptional regulation remains unclear; studies disrupting chromatin loops comprehensively throughout the genome have produced mixed results (Rao et al., 2017; Schwarzer et al., 2017; Cuartero et al., 2018; Stik et al., 2020). Ablation of loops in the human colorectal cancer cell line HCT-116 only altered the expression of a handful of genes (Rao et al., 2017). In contrast, loss of loops in murine liver cells and macrophages responding to LPS induced thousands of transcriptional changes (Schwarzer et al., 2017; Cuartero et al., 2018; Stik et al., 2020). Differences in biological systems, cellular contexts, and even the method of loop disruption could potentially explain the conflicting findings.

We investigated our data to see whether it supported a role of looping in gene regulation in response to external stimuli. Our analyses were based on the assumption that, if loops play a role in transcriptional control, then looped enhancer-gene pairs should exhibit correlated changes in histone H3K27ac and gene expression. Because only a small fraction of loops change over time, all loops were used to connect enhancers to promoters regardless of differential status. In total, this involved 5,039 enhancer-promoter loops featuring 4,093 unique genes, 1,483 of which were differential. In total, 25.4% of differential genes were connected to a distal enhancer via a chromatin loop. We investigated the temporal patterns of these looped enhancer-promoter pairs and compared them with sets of non-looped enhancer-promoter pairs of similar genomic distance (base pairs) or contact frequency (Hi-C measurements). These matched non-looped sets were identified using the matchRanges function available from the nullranges R/Bioconductor package (Figure 2A; Davis et al., 2022). Because of the absence of long-range chromatin loops at these enhancer-promoter pairs, contact-matched pairs had Hi-C contact frequencies similar to looped pairs but were much closer in base pairs (Figure 2B, dark gray). In contrast, distance-matched pairs were separated by a similar number of base pairs as the looped pairs but had much lower Hi-C contact frequencies (Figure 2B, light gray). Comparisons between these non-looped matched sets and the looped enhancer-promoter pairs allowed us to isolate the effect of contact frequency and distance independently and investigate the additional effect of chromatin looping by adjusting for these features.

To explore the correlation of enhancers and genes over time, we clustered our differential genes based on the time point when they exhibited their maximal up- or downregulation with respect to the 0 h time point and plotted their average normalized expression (Figure 2C, yellow lines). Only clusters peaking at intermediate time points and with more than 100 genes are shown. For each gene cluster, we identified enhancers that were connected to those genes via a chromatin loop and plotted their average normalized histone H3K27ac signal (Figure 2C, red lines). All 6 clusters revealed a clear correlation between histone H3K27ac and gene expression at looped enhancer-promoter pairs, supporting the idea that looped pairs are functionally

connected. Interestingly, the changes in acetylation preceded changes in gene expression by 30–60 min. This lag is also seen in changes in promoter acetylation (Figure S3A, black lines), and is consistent with enhancer activation causing changes to gene expression.

Despite this evidence, it is important to consider that chromatin loops occur over relatively short distances (median, ~390 kb), and at such short distances, even non-looped enhancers and promoters exhibit elevated chromatin contact frequencies compared with randomly selected enhancers and genes across the genome. Therefore, the correlation between looped enhancers and promoters we observe could be explained by genomic distance alone. To determine whether looped enhancer-promoter pairs exhibited higher correlation than expected given their genomic distance, we compared looped enhancer-promoter pairs with non-looped enhancer-promoter pairs that were matched for genomic distance (Figure 2A). Distance-matched, non-looped enhancer-promoter pairs exhibited some degree of correlation (Figure 2C, light gray lines); however, the correlation was weaker than that observed at looped enhancer-promoter pairs. Thus, distance alone does not account for the enhancer-promoter correlations observed at loop anchors and offers further support for the functional role of loops in enhancer-based gene regulation.

One explanation for how loops exhibit transcriptional control is by increasing contact frequencies between enhancers and their target genes. To determine whether looped enhancer-promoter pairs exhibited a higher correlation than expected given their contact frequency, we compared looped enhancer-promoter pairs to non-looped enhancer-promoter pairs that were matched for contact frequency. Surprisingly, although contact-matched pairs exhibited a stronger correlation than distance-matched pairs, the correlation was still weaker than that observed at looped enhancer-promoter pairs (Figure 2C, dark gray lines). We confirmed these results using data from our previously published study of monocyte differentiation (Figures S3B and S3C; Phanstiel et al., 2017). There too, looped enhancer-promoter pairs exhibited better correlation than enhancer-promoter pairs that were matched for distance or contact frequency. This was surprising and suggests that the presence of a chromatin loop may facilitate a functional regulatory connection through mechanisms beyond simply increasing their frequency of physical proximity. We explore some possible explanations for this in the discussion.

## Changes in gene expression exhibit a directional bias at differential loop anchors

Given the correlation we observed between acetylation and gene expression at opposite ends of chromatin loops, we hypothesized that changes in looping would be associated with altered transcription of genes at loop anchors and that the directionality of changes in expression would match that of the changes in looping. To test this, we used k-means clustering to identify four categories of differential looping: gained early, gained late, lost early, and lost late. Generally, "early" differential loops changed within the first 2 h of treatment, whereas "late" differential loops did not change until 4 h or beyond, many unique to the 24-h time point. Examples of loops from each cluster are shown in Figure 3A. Differential loops spanned approximately 170–200 kb on average, with the exception of gained late loops, which were much larger with an average length of 610 kb (Figure S4A). Compartmental analysis revealed that these gained late loops were also closer to the B compartment than other differential loop classes (Figure S4B). Although all loops on average fall into the more transcriptionally active A compartment, differential loops shifted farther to the A compartment over the course of activation.

Next we calculated the percentage of genes at each set of loop anchors that were significantly up- or downregulated in response to LPS + $IFN_\gamma$ treatment (Figures 3B, S4C, and D). Anchor genes were defined by overlapping gene promoters with loop anchors (STAR Methods). Gained loop anchors were enriched for the promoters of upregulated genes (permutation test, $n = 10{,}000$, $p < 0.05$) and shifted toward the A compartment during treatment (Figure S4B). These observations are consistent with findings from previous work by our lab and others that have associated increased looping with increased transcription of anchor genes (Rao et al., 2014; Phanstiel et al., 2017) and generally support a causal role of looping in transcriptional control. However, lost loops were also associated with increased transcription of anchor genes and a shift toward the A compartment (permutation test, $n = 10{,}000$, $p < 0.05$). Although surprising, this is consistent with data from Rao et al., (2017) that showed that removal of DNA loops is not necessarily accompanied by decreased transcription of anchor genes.

To explore this further, we separately analyzed anchor gene expression based on whether genes were oriented toward or away from the center of the loop. Intriguingly, genes at the anchors of gained and lost loop classes exhibited different directional biases (Figures 3C and S4E). At gained loops, outward-oriented anchor genes exhibited significantly more increased expression than inward-oriented genes (Wilcoxon rank-sum test, $p < 0.05$). In contrast, at lost loops, inward-oriented anchor genes exhibited more increased expression than outward-oriented genes (Wilcoxon rank-sum test, $p < 0.05$). Similar trends can be seen using differential loops from monocyte-to-macrophage differentiation (Figure S4F). To investigate this further, we examined the temporal profiles of differential loops and anchor genes. For each loop cluster, we calculated the average fold change of inward- and outward-facing anchor genes (Figure 3D). At gained loops, the contact frequency and transcription of anchor genes were positively correlated over time, particularly for loops oriented away from the center of the loop. The gained early loops exhibited increased contact frequency 30–60 min prior to the increased transcription of outward-oriented anchor genes, which is consistent with the notion of loops playing a causal role in gene expression. We see a similar lag between increases in compartment and transcription on a coarser level (Figure S5). The gained late loops showed correlated changes in outward-oriented anchor gene expression, but because they changed most drastically between 6 and 24 h, the time points were not close enough to observe a temporal lag. In contrast, at lost loops, contact frequency and transcription of anchor genes were inversely correlated, particularly for loops oriented toward the center of the loop.

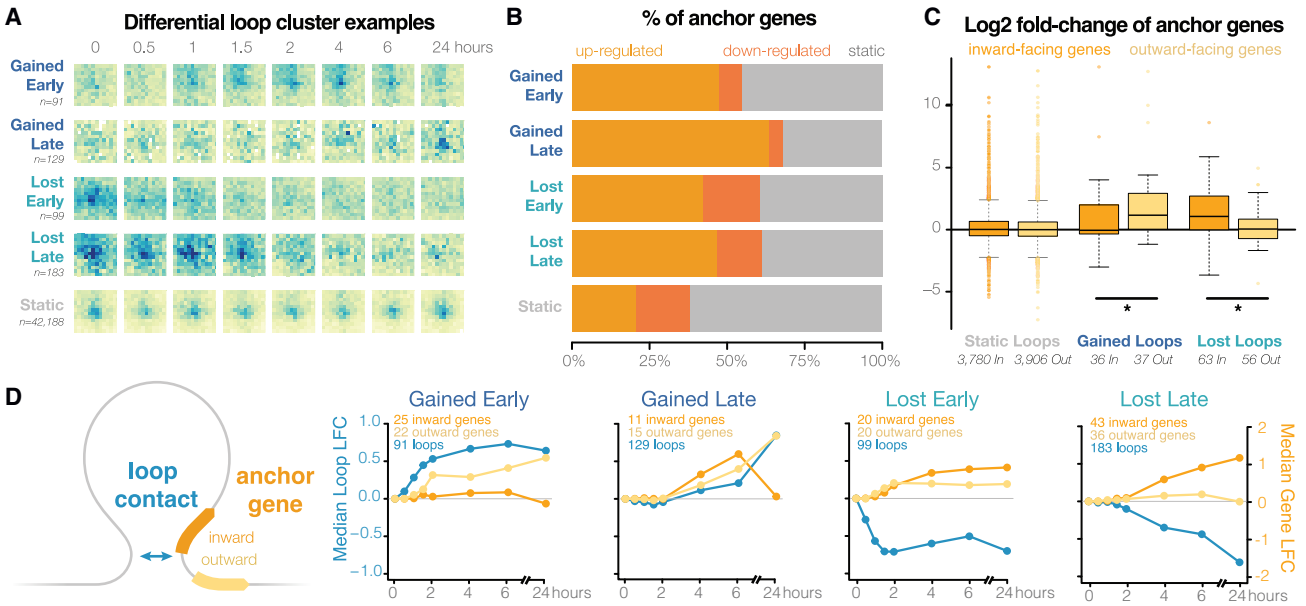


**Figure 3. Upregulated genes anchored at differential loops exhibit directionality bias**

(A) 502 differential loops were clustered (k-means) according to their timing and direction. Generally, "early" changes occurred within the first 2 h, and "late" changes occurred within 4 h and beyond. Representative loops are shown for each cluster (5-kb resolution).

(B) The anchors in all differential loop clusters are enriched for upregulated genes.

(C) Distributions of log2 fold changes of genes with promoters in the anchors of static and differential loops. Anchor genes were classified by whether they are oriented toward (inward, orange) or away from (outward, yellow) the center of the loop. Among genes at gained loop anchors, the fold change of outward-facing genes is significantly higher than of inward-facing genes, whereas the opposite trend is seen among genes at lost loops (Wilcoxon rank-sum test, $p < 0.05$).

(D) Average log2 fold change of differential loops (blue) and inward- and outward-facing genes (orange, yellow) with promoters overlapping those loop anchors.

## Lost loops are associated with high levels of transcription within loop boundaries

One possible explanation for the directional biases we observe at differential loop anchors is that transcription may be antagonistic to loop extrusion and that high levels of transcription at loop anchors, or within the loop itself, may destabilize loop extrusion complexes. This would agree with several previous studies highlighting the ability of RNAP to push and/or displace cohesin (Busslinger et al., 2017; Heinz et al., 2018).

To determine whether antagonism between transcription and loop extrusion could explain the increased expression we observed at lost loop anchors, we explored the absolute and relative levels of transcription occurring within the boundaries of differential loops. As with anchor genes, the sets of genes within the bounds of loops of the various clusters were largely unique, with minimal overlap (Figures S4G and S4H). Because the majority of transcription occurs at introns, which are generally not captured in our RNA-seq data, we devised an inferred transcription score (ITS) to roughly estimate the levels of transcription for every 10-kb bin in the genome using our RNA-seq data (STAR Methods). Briefly, the transcript per million (TPM) value for each gene was assigned to every genomic bin covered by the gene body. Values were summed for bins that overlapped multiple genes.

Using our ITSs, we observed that gained loops have relatively low levels of internal transcription at all time points (average ITS $\leq 50$; Figure 4A). In contrast, decreasing loops achieved much higher average levels of internal transcription during the time course (Figure 4A; ITS > 50 at most time points), and the amount of internal transcription is inversely correlated with changes in loop strength ($R^2$ is $-0.59$ for lost early and $-0.99$ for lost late loops). To determine how big of a change in ITS was required to observe a decrease in loop strength, we explored how the changes in ITS within a loop correlated with loop fold change. Loops with a mean increase in ITS of 10 or more exhibited a statistically significant decrease in loop strength (Wilcoxon signed-rank test, $p < 0.01$; Figure 4B). Visualizing transcription relative to the loop boundaries (Figure 4C) confirmed these findings. Transcription was enriched outside of the boundaries of gained loops (in the 50 kb upstream of the upstream anchors, or downstream from the downstream anchors). In contrast, transcription was enriched between the anchors of lost loops, within the loop bounds. These data are consistent with a model in which high levels of transcription antagonize loop extrusion.

This suggests that the causal arrow between looping and transcription might point both ways: DNA loop formation may contribute to increased transcription of target genes, but very high levels of transcription could contribute to the weakening loops by antagonizing loop extrusion, as observed previously (Busslinger et al., 2017; Heinz et al., 2018; Brandão et al., 2019; Gu et al., 2020; Banigan et al., 2022; Leidescher et al., 2022). An example of these potential phenomena can be seen at the *GBP* locus (Figure 5A; see Figure S6 for other examples). In untreated cells, seven *GBP* genes are encompassed by two large (370- and 470-kb) "structural" loops whose anchors do not overlap active gene promoters. Small loops start to form as

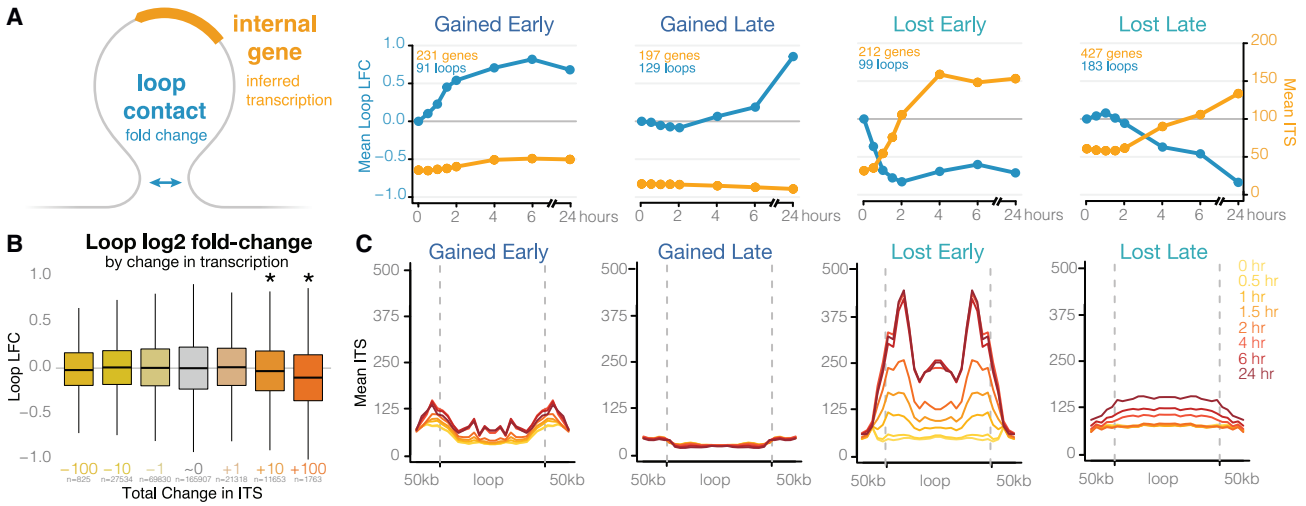


**Figure 4. Lost loops are characterized by high levels of internal transcription**

(A) Log2 fold change of differential loops (blue) and average internal inferred transcription score (ITS; gold) for loops of each cluster. Gained loops have lower levels of internal transcription than lost loops, and the temporal dynamics of changes in transcription are anti-correlated with changes in loop strength among lost loops. For each loop, ITS was calculated and averaged across 2 biological replicates.

(B) Binning loops based on their change in internal transcription shows significant weakening of loops that gain 10 or more ITSs per 10 kb (Wilcoxon signed-rank test, $p < 10^{-20}$).

(C) Average ITS within and 50 kb beyond loop boundaries. Transcription is highest at and beyond loop anchors in gained early loops, low among gained late loops, and localized within loop bounds in lost loops.

early as 30 min after activation, connecting H3K27ac peaks to promoters. This is followed by increased expression of genes at the anchors of those loops. This increased expression is coupled with loss of the large structural loops that span this locus. Visualizing these changes via line plots (Figures 5B–5E) highlights the correlation between looping and anchor gene transcription as well as the inverse correlation between structural loops and internal transcription.

## DISCUSSION

### Temporal analysis of macrophage activation

We used a fine-scale multi-omics time course of macrophage activation and quantified changes in DNA looping, enhancer acetylation, and gene expression. The high temporal resolution of the Hi-C data revealed changes in chromatin looping along short, transcriptionally relevant time scales that were undetected at time course endpoints. Combining the data across time points yielded Hi-C data at a depth of over 16 billion contacts, allowing sensitive and robust detection of macrophage chromatin loops. Integration of the data revealed several findings regarding the nature of DNA loops.

### The influence of chromatin structure on transcription

The correlated changes we observe between looped enhancers and promoters are consistent with loops serving as a functional bridge between enhancers and their target genes, at least for genes regulated in response to external stimuli. This is supported by temporal ordering of events that reveal that loop formation and looped-enhancer activation occur prior to increases in anchor gene expression. This agrees with a previous study of cells responding to glucocorticoids in which maximal changes in loops were observed earlier than maximal changes in genes (D'Ippolito et al., 2018). These results are somewhat inconsistent with results from Rao et al. (2017), which showed very few changes in gene expression in response to global loop disruption via RAD21 degradation (Rao et al., 2017); however, in that study, the cells were grown in steady state and not responding to external stimuli. In experimental designs more comparable with ours, cohesin or CTCF depletion did disrupt the transcriptional response of macrophages to microbial stimuli (Cuartero et al., 2018; Stik et al., 2020). This suggests that loops likely play a critical role in mediating transcriptional changes in cellular response to stimuli.

Intriguingly, we found that non-looped enhancer-promoter pairs that were matched for contact frequency and histone H3K27ac levels did not exhibit the same level of temporal correlation as looped enhancer-promoter pairs. This suggests that loops may exert their regulatory control via mechanisms beyond merely increasing contact frequency between enhancers and promoters. One possible but speculative explanation is that activation of transcription by distal enhancers may require prolonged enhancer-promoter contact rather than overall contact frequency. Transcription factor binding is typically quite transient (Lu and Lionnet, 2021), and prolonged contact might be required for proper formation of enhancer, polymerase, or mediator complexes that drive transcriptional activation. Recent work using 3D super-resolution live-cell imaging found that loops stabilized contact between anchors for 10–30 min (Gabriele et al., 2021). In the absence of a chromatin loop, such prolonged contact is unlikely even for non-looped enhancers and promoters that are separated by relatively short genomic distances. Closely spaced

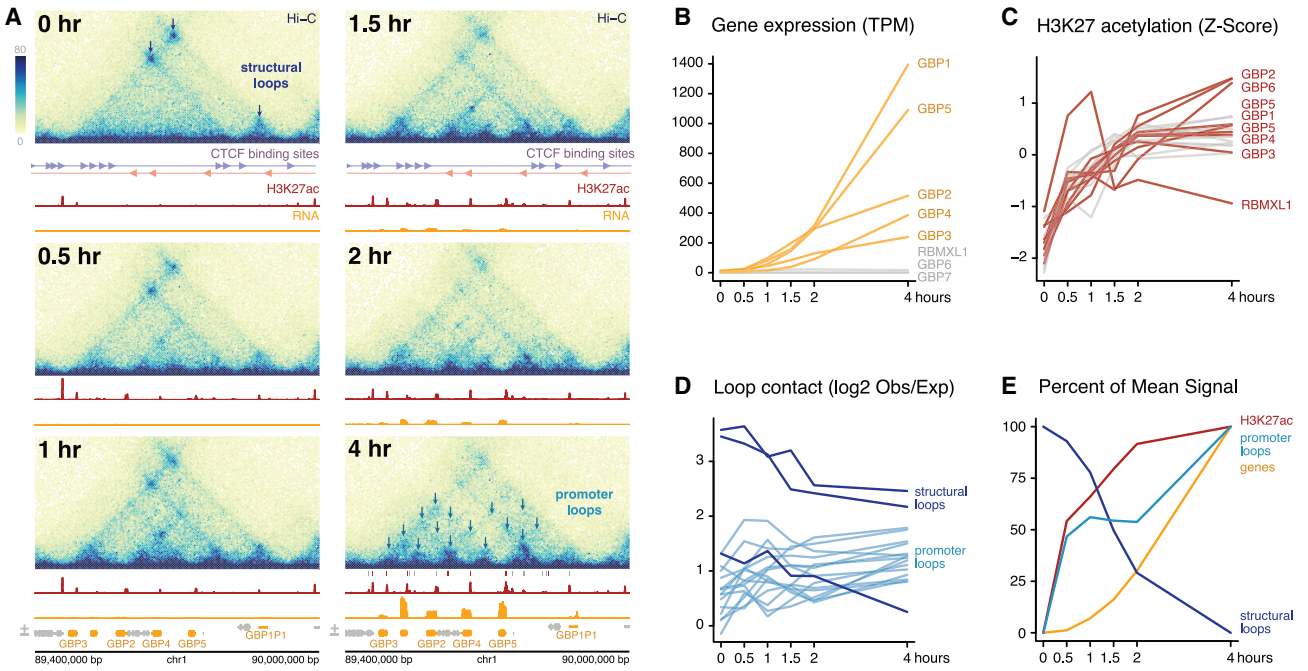


**Figure 5. Long-distance loops are lost concurrently with increased internal transcription and restructuring at the *GBP* locus**

(A) Chromatin structure (5-kb resolution), H3K27 acetylation, and gene transcription change drastically over the first 4 h at the *GBP* locus of chromosome 1. Predicted CTCF binding sites are also shown. Prior to treatment, two large "structural" loops (not connecting enhancers and promoters) encompass several *GBP* genes. After 30–60 min of LPS/IFN$_\gamma$ treatment, *GBP* promoters become acetylated. From 1 h onward, as acetylation increases, connections form between the *GBP* promoters. As genes become more highly expressed at 1.5 h and beyond, the original long-distance structural loops weaken in favor of shorter-range, transcription-correlated contacts. Hi-C scale is indicated in KR-normalized counts.

(B) The TPM of each gene in the region, with the up-regulated genes highlighted in yellow (as in A).

(C) The *Z* score-normalized change in H3K27ac at promoters (red) and putative enhancers (gray) in this region. The promoters and enhancers plotted are highlighted in the 4-h panel in (A).

(D) The log-transformed ratio of observed to expected contact frequency of several points in the region. "Structural" loops (as in A, 0 h) are colored dark blue, and promoter-promoter and promoter-enhancer loops (as in A, 4 h) are colored light blue.

(E) The mean TPM (for expressed genes), *Z* score (for H3K27ac), and log2 observed/expected ratio (for structural or promoter contacts) for the individual features highlighted in (B)–(D).

but non-looped enhancer-promoter pairs might participate in much more frequent but shorter-duration contacts that are insufficient for transcriptional activation. Hi-C data measure contact frequency but cannot differentiate between frequent short interactions and infrequent but prolonged interactions. Further exploration is required to determine whether prolonged contacts do indeed account for these differences and, if so, what the exact mechanisms are.

These observations are consistent with many possible models of long-range enhancer activity, including those that require stable or transient contact (also called "hit-and-run" or "kissing" models) (Brandão et al., 2021; Karr et al., 2022). We see gained transcription at not just *de novo* but also quantitatively strengthened loops, which is consistent with a model where modest enhancer contact coupled with futile cycles of promoter activity could result in large effects on transcription (Xiao et al., 2021). This futile cycle model also predicts a lag between changes in loop strength and transcription but on a longer timescale than we observed. Other models, such as the transcription factor activity gradient (TAG) model, suggest that proximity rather than direct contact is required for long-range regulation (Karr et al., 2022). Although such a model could also support looped enhancers regulating distal promoters, it would require promoter-specific activities to explain how non-looped enhancers in equal contact frequency are not as strongly regulated.

## The influence of transcription on chromatin structure

Several analyses from this paper support a model in which high levels of transcription could stall, displace, or generally antagonize loop extrusion complexes. First, we found that changes in gene expression exhibit a directional bias at differential loop anchors. The anchors of gained enhancer-promoter loops were associated with increased gene expression of genes oriented away from the center of the loop but not genes oriented toward the center of the loop. In contrast, lost enhancer-promoter loops were associated with increased expression of anchor genes oriented toward the center of the loop but not those oriented away from it. The temporal patterns of loop loss and internal transcription were anti-correlated, although, when averaging across all lost loops, the temporal order is not as obvious as the trends seen among gained loops, which more clearly precede transcriptional

changes. These temporal analyses agree with previous work showing accumulation of cohesin at the 3′ ends of genes in a manner correlated with the amount of transcription and also sensitive to transcriptional inhibition (Busslinger et al., 2017; Heinz et al., 2018; Olan et al., 2020) and recent studies demonstrating that RNAP may act as a "moving barrier" to loop extrusion (Banigan et al., 2022). Transcription may also shape chromatin independent of cohesin. Recent high-resolution microscopy and Micro-C experiments have detected fine-scale cohesin-independent structures between and within highly expressed genes, which could compete with or disrupt cohesin-mediated structures (Hsieh et al., 2020; Leidescher et al., 2022). Transcription inhibition interrupts these local structures but leaves intact broader loops, domains, and compartments. Virtually all transcriptionally active chromatin exhibits elevated contact frequency via a phenomenon called compartmentalization that does not require cohesin (Rao et al., 2017; Rowley and Corces, 2018; Vian et al., 2018). It remains possible that such compartmentalization itself could disrupt loops surrounding highly expressed genes.

Finally, lost loops were associated with relatively high levels of internal transcription, and only very large changes in transcription were associated with decreased looping. This might reflect the fact that, in most cases, collisions between transcription and loop extrusion are rare. Indeed, transcription occurs in relatively infrequent bursts (Fukaya et al., 2016), and loops appear to spend at least some time in fully looped or fully non-looped states (Gabriele et al., 2021). So at low to moderate levels of transcription, collisions might be uncommon and are not a major driver of 3D chromatin structure. So perhaps it is only at extremely high levels of transcription where such collisions are frequent enough to lead to observable losses in loop-based contacts. Alternatively, it is possible that transcription only slightly impedes extrusion and that at low levels of transcription, changes in contact frequency are imperceptible. This agrees with studies showing that transcription briefly stalls condensin translocation but that it only measurably affects 3D chromatin structures at extremely highly expressed loci, such as at rRNA genes (Brandão et al., 2019).

### Future directions

This fine-scale time course of looping in human macrophages provides insight into the temporal organization of regulatory events in human cells responding to external stimuli and a deeper understanding of the mechanisms driving transcriptional regulation in human cells. Some of the findings could be useful for predicting functional enhancer-promoter pairs. For example, the temporally coordinated changes observed at looped enhancer-promoter pairs could be employed to refine and potentially improve predictions made by the activity-by-contact model (Fulco et al., 2019).

This work supports a model in which loop extrusion and transcription participate in a coordinated dance and can influence each other in a reciprocal relationship. If this holds true, then it could have important implications for how genes are organized in the context of chromatin loops. For example, genes oriented toward the center of a loop could be regulated by a negative feedback mechanism in which high levels of transcription might decrease looping between the promoter and a distal enhancer. Moving forward, incorporation of more data types into these time courses should reveal further insights into the mechanisms of 3D chromatin structure and gene regulation.

### Limitations of the study

This paper aimed to place genomic events in temporal order, but several caveats should be considered based on the methods used. RNA-seq measures accumulation of transcribed RNA but does not directly measure the amount of transcription along the genome. Our ITS, calculated by expanding TPM counts across gene bodies including introns, was used as a proxy, but alternative methods, such as precision nuclear run-on sequencing (PRO-Seq) or global run-on sequencing (GRO-Seq), would be required to directly measure this. Use of bulk methods in independent cell populations provided high sample numbers and allowed us to view general trends, but it means that we are only able to detect how changes correlate on a population level and cannot determine how events are co-occurring in individual cells. Finally, additional time points would provide further insights into the changes observed here. For example, evenly spaced time points of every 30 min would reduce extrapolation and improve temporal correlation assessments. Similarly, more closely spaced timepoints could reveal even finer-scale lags in temporal trends but could be more logistically challenging for high-throughput methods. Other studies implementing single-cell techniques could complement these limitations nicely and would be interesting to compare with the trends observed here.

## STAR★METHODS

Detailed methods are provided in the online version of this paper and include the following:

- KEY RESOURCES TABLE
- RESOURCE AVAILABILITY
  - Lead contact
  - Materials availability
  - Data and code availability
- EXPERIMENTAL MODEL AND SUBJECT DETAILS
  - Cell lines
- METHOD DETAILS
  - Macrophage differentiation and activation
  - Crosslinking
  - RNA-seq library preparation
  - ChIP-seq library preparation
  - *In situ* Hi-C library preparation
  - ATAC-seq library preparation
- QUANTIFICATION AND STATISTICAL ANALYSIS
  - RNA-seq processing and gene quantification
  - Inferred transcription score (ITS) calculations
  - ATAC- and ChIP-seq processing and peak calling
  - Enhancer and promoter definitions
  - Predicted CTCF binding sites
  - Hi-C processing, loop and compartment calling
  - Differential gene and peak analysis
  - Differential loop analysis and clustering
  - Matched enhancer-promoter sets

## SUPPLEMENTAL INFORMATION

Supplemental information can be found online at https://doi.org/10.1016/j.celrep.2022.111567.

## ACKNOWLEDGMENTS

We thank Erika Deoudes for data visualization, illustration, proofreading, and typesetting. We thank Samantha Pattenden for use of the Covaris LE220 instrument, which was provided by North Carolina Biotechnology Center Institute Development Program grant 2017-IDG-1005. We thank Samantha Pattenden and Paul Dayton for generously supplying the nanodroplets used for chromatin shearing (Triangle Biotechnology, FF101-5000, Durham, NC). This work was supported by NIH grants (R35-GM128645 to D.H.P., R00HG008662 to D.H.P., R35GM143532 to I.H., and R01AG066871 to H.W.) and multiple NIH training grants (T32-GM067553 to E.S.D., T32 GM007092 to K.S.M.R. and E.T., and T32 GM135128 to M.L.B.). I.Y.Q. was supported by a BrightFocus Foundation postdoctoral fellowship. I.H. was supported by an award from the Cancer Prevention & Research Institute of Texas (RR170030). E.S.D. and M.I.L. were supported by a CZI Essential Open Source Software for Science (EOSS) Round 3 award.

## AUTHOR CONTRIBUTIONS

K.S.M.R. designed and performed the majority of experiments, performed computational analysis, and wrote the paper. E.S.D. developed software and performed computational analyses. M.L.B. performed some cell culture and genomic library preparation experiments. A.C. performed some cell culture experiments. E.T. performed some cell culture experiments and assisted with ChIP-seq. I.Y.Q. prepared ATAC-seq libraries. S.C. helped prepare ATAC-seq libraries and ChIP-seq cross-linking. K.T.W. assisted with cell culture experiments. H.W. supervised and helped interpret genomics data. I.H. oversaw the planning, supervision, and interpretation of some experiments. M.I.L. supervised computational analyses and software development. D.H.P. acquired funding, conceptualized the project, supervised experiments and data analyses, and helped write the paper.

## DECLARATION OF INTERESTS

The authors declare no competing interests.

Received: May 18, 2022
Revised: August 19, 2022
Accepted: October 5, 2022
Published: November 1, 2022

## REFERENCES

Abramo, K., Valton, A.L., Venev, S.V., Ozadam, H., Fox, A.N., and Dekker, J. (2019). A chromosome folding intermediate at the condensin-to-cohesin transition during telophase. Nat. Cell Biol. *21*, 1393–1402.

Ahn, J.H., Davis, E.S., Daugird, T.A., Zhao, S., Quiroga, I.Y., Uryu, H., Li, J., Storey, A.J., Tsai, Y.H., Keeley, D.P., et al. (2021). Phase separation drives aberrant chromatin looping and cancer development. Nature *595*, 591–595.

Akdemir, K.C., Le, V.T., Chandran, S., Li, Y., Verhaak, R.G., Beroukhim, R., Campbell, P.J., Chin, L., Dixon, J.R., Futreal, P.A., et al. (2020). Disruption of chromatin folding domains by somatic genomic rearrangements in human cancer. Nat. Genet. *52*, 294–305.

Andrews, S.; Babraham Bioinformatics (2010). FastQC: A quality control tool for high throughput sequence data 0.11.5. https://www.bioinformatics.babraham.ac.uk/projects/fastqc/.

Arner, E., Daub, C.O., Vitting-Seerup, K., Andersson, R., Lilje, B., Drabløs, F., Lennartsson, A., Rönnerblad, M., Hrydziuszko, O., Vitezic, M., et al. (2015). Transcribed enhancers lead waves of coordinated transcription in transitioning mammalian cells. Science *347*, 1010–1014.

Krueger, F.; Babraham Bioinformatics (2015). Trim Galore! 0.4.3. http://www.bioinformatics.babraham.ac.uk/projects/trim_galore/.

Banigan, E.J., Tang, W., van den Berg, A.A., Stocsits, R.R., Wutz, G., Brandão, H.B., Busslinger, G.A., Peters, J.M., and Mirny, L.A. (2022). Transcription shapes 3D chromatin organization by interacting with loop-extruding cohesin complexes. Preprint at bioRxiv. https://doi.org/10.1101/2022.01.07.475367.

Beagan, J.A., Pastuzyn, E.D., Fernandez, L.R., Guo, M.H., Feng, K., Titus, K.R., Chandrashekar, H., Shepherd, J.D., and Phillips-Cremins, J.E. (2020). Three-dimensional genome restructuring across timescales of activity-induced neuronal gene expression. Nat. Neurosci. *23*, 707–717.

Bertero, A., Fields, P.A., Ramani, V., Bonora, G., Yardimci, G.G., Reinecke, H., Pabon, L., Noble, W.S., Shendure, J., and Murry, C.E. (2019). Dynamics of genome reorganization during human cardiogenesis reveal an RBM20-dependent splicing factory. Nat. Commun. *10*, 1538.

Bonev, B., Mendelson Cohen, N., Szabo, Q., Fritsch, L., Papadopoulos, G.L., Lubling, Y., Xu, X., Lv, X., Hugnot, J.P., Tanay, A., and Cavalli, G. (2017). Multiscale 3D genome rewiring during mouse neural development. Cell *171*, 557–572.e24.

Brandão, H.B., Paul, P., van den Berg, A.A., Rudner, D.Z., Wang, X., and Mirny, L.A. (2019). RNA polymerases as moving barriers to condensin loop extrusion. Proc. Natl. Acad. Sci. USA *116*, 20489–20499.

Brandão, H.B., Gabriele, M., and Hansen, A.S. (2021). Tracking and interpreting long-range chromatin interactions with super-resolution live-cell imaging. Curr. Opin. Cell Biol. *70*, 18–26.

Buenrostro, J.D., Giresi, P.G., Zaba, L.C., Chang, H.Y., and Greenleaf, W.J. (2013). Transposition of native chromatin for fast and sensitive epigenomic profiling of open chromatin, DNA-binding proteins and nucleosome position. Nat. Methods *10*, 1213–1218.

Busslinger, G.A., Stocsits, R.R., van der Lelij, P., Axelsson, E., Tedeschi, A., Galjart, N., and Peters, J.M. (2017). Cohesin is positioned in mammalian genomes by transcription, CTCF and Wapl. Nature *544*, 503–507.

Corces, M.R., Trevino, A.E., Hamilton, E.G., Greenside, P.G., Sinnott-Armstrong, N.A., Vesuna, S., Satpathy, A.T., Rubin, A.J., Montine, K.S., Wu, B., et al. (2017). An improved ATAC-seq protocol reduces background and enables interrogation of frozen tissues. Nat. Methods *14*, 959–962.

Cuartero, S., Weiss, F.D., Dharmalingam, G., Guo, Y., Ing-Simmons, E., Masella, S., Robles-Rebollo, I., Xiao, X., Wang, Y.F., Barozzi, I., et al. (2018). Control of inducible gene expression links cohesin to hematopoietic progenitor self-renewal and differentiation. Nat. Immunol. *19*, 932–941.

Danecek, P., Bonfield, J.K., Liddle, J., Marshall, J., Ohan, V., Pollard, M.O., Whitwham, A., Keane, T., McCarthy, S.A., Davies, R.M., and Li, H. (2021). Twelve years of SAMtools and BCFtools. GigaScience *10*, giab008. https://doi.org/10.1093/gigascience/giab008.

Davidson, I.F., Goetz, D., Zaczek, M.P., Molodtsov, M.I., Huis In 't Veld, P.J., Weissmann, F., Litos, G., Cisneros, D.A., Ocampo-Hafalla, M., Ladurner, R., et al. (2016). Rapid movement and transcriptional re-localization of human cohesin on DNA. EMBO J. *35*, 2671–2685.

Davis, E.S., Mu, W., Lee, S., Dozmorov, M.G., Love, M.I., and Phanstiel, D.H. (2022). matchRanges: generating null hypothesis genomic ranges via covariate-matched sampling. Preprint at bioRxiv. https://doi.org/10.1101/2022.08.05.502985.

Dekker, J., Rippe, K., Dekker, M., and Kleckner, N. (2002). Capturing chromosome conformation. Science *295*, 1306–1311.

Dekker, J., and Mirny, L. (2016). The 3D genome as moderator of chromosomal communication. Cell *164*, 1110–1121.

D'Ippolito, A.M., McDowell, I.C., Barrera, A., Hong, L.K., Leichter, S.M., Bartelt, L.C., Vockley, C.M., Majoros, W.H., Safi, A., Song, L., et al. (2018). Pre-established chromatin interactions mediate the genomic response to glucocorticoids. Cell systems *7*, 146–160.e7.

Dostie, J., Richmond, T.A., Arnaout, R.A., Selzer, R.R., Lee, W.L., Honan, T.A., Rubio, E.D., Krumm, A., Lamb, J., Nusbaum, C., et al. (2006). Chromosome Conformation Capture Carbon Copy (5C): a massively parallel solution for

mapping interactions between genomic elements. Genome Res. *16*, 1299–1309.

Dozmorov, M.G., Davis, E., Mu, W., Lee, S., Triche, T., Phanstiel, D., and Love, M. (2022–). CTCF - R package version 0.99.5 0.99.5. https://github.com/mdozmorov/CTCF.

Durand, N.C., Robinson, J.T., Shamim, M.S., Machol, I., Mesirov, J.P., Lander, E.S., and Aiden, E.L. (2016). Juicebox provides a visualization system for Hi-C contact maps with unlimited zoom. Cell Syst. *3*, 99–101.

Ewels, P., Magnusson, M., Lundin, S., and Käller, M. (2016). MultiQC: summarize analysis results for multiple tools and samples in a single report. Bioinformatics *32*, 3047–3048.

Fukaya, T., Lim, B., and Levine, M. (2016). Enhancer control of transcriptional bursting. Cell *166*, 358–368.

Fulco, C.P., Nasser, J., Jones, T.R., Munson, G., Bergman, D.T., Subramanian, V., Grossman, S.R., Anyoha, R., Doughty, B.R., Patwardhan, T.A., et al. (2019). Activity-by-contact model of enhancer-promoter regulation from thousands of CRISPR perturbations. Nat. Genet. *51*, 1664–1669.

Fullwood, M.J., Liu, M.H., Pan, Y.F., Liu, J., Xu, H., Mohamed, Y.B., Orlov, Y.L., Velkov, S., Ho, A., Mei, P.H., et al. (2009). An oestrogen-receptor-alpha-bound human chromatin interactome. Nature *462*, 58–64.

Furlan-Magaril, M., Ando-Kuri, M., Arzate-Mejía, R.G., Morf, J., Cairns, J., Román-Figueroa, A., Tenorio-Hernández, L., Poot-Hernández, A.C., Andrews, S., Várnai, C., et al. (2021). The global and promoter-centric 3D genome organization temporally resolved during a circadian cycle. Genome Biol. *22*, 162.

Gabriele, M., Brandão, H.B., Grosse-Holz, S., Jha, A., Dailey, G.M., Cattoglio, C., Hsieh, T.H.S., Mirny, L., Zechner, C., and Hansen, A.S. (2021). Dynamics of CTCF and cohesin mediated chromatin looping revealed by live-cell imaging. Preprint at bioRxiv. https://doi.org/10.1101/2021.12.12.472242.

Gu, B., Comerci, C.J., McCarthy, D.G., Saurabh, S., Moerner, W.E., and Wysocka, J. (2020). Opposing effects of cohesin and transcription on CTCF organization revealed by super-resolution imaging. Mol. Cell *80*, 699–711.e7.

Hahsler, M., Piekenbrock, M., and Doran, D. (2019). dbscan: fast density-based clustering with R. J. Stat. Software *91*, 1–30. https://doi.org/10.18637/jss.v091.i01.

Heidari, N., Phanstiel, D.H., He, C., Grubert, F., Jahanbani, F., Kasowski, M., Zhang, M.Q., and Snyder, M.P. (2014). Genome-wide map of regulatory interactions in the human genome. Genome Res. *24*, 1905–1917.

Heinz, S., Texari, L., Hayes, M.G.B., Urbanowski, M., Chang, M.W., Givarkes, N., Rialdi, A., White, K.M., Albrecht, R.A., Pache, L., et al. (2018). Transcription elongation can affect genome 3D structure. Cell *174*, 1522–1536.e22.

Hsieh, T.-H.S., Cattoglio, C., Slobodyanyuk, E., Hansen, A.S., Rando, O.J., Tjian, R., and Darzacq, X. (2020). Resolving the 3D landscape of transcription-linked mammalian chromatin folding. Mol. Cell *78*, 539–553.e8.

Johnstone, S.E., Reyes, A., Qi, Y., Adriaens, C., Hegazi, E., Pelka, K., Chen, J.H., Zou, L.S., Drier, Y., Hecht, V., et al. (2020). Large-scale topological changes restrain malignant progression in colorectal cancer. Cell *182*, 1474–1489.e23.

Karr, J.P., Ferrie, J.J., Tjian, R., and Darzacq, X. (2022). The transcription factor activity gradient (TAG) model: contemplating a contact-independent mechanism for enhancer-promoter communication. Genes Dev. *36*, 7–16.

Kasoji, S.K., Pattenden, S.G., Malc, E.P., Jayakody, C.N., Tsuruta, J.K., Mieczkowski, P.A., Janzen, W.P., and Dayton, P.A. (2015). Cavitation enhancing nanodroplets mediate efficient DNA fragmentation in a bench top ultrasonic water bath. PLoS One *10*, e0133014.

Kim, D., Paggi, J.M., Park, C., Bennett, C., and Salzberg, S.L. (2019). Graph-based genome alignment and genotyping with HISAT2 and HISAT-genotype. Nat. Biotechnol. *37*, 907–915.

Lee, J., Krivega, I., Dale, R.K., and Dean, A. (2017). The LDB1 complex Co-opts CTCF for erythroid lineage-specific long-range enhancer interactions. Cell Rep. *19*, 2490–2502.

Leidescher, S., Ribisel, J., Ullrich, S., Feodorova, Y., Hildebrand, E., Galitsyna, A., Bultmann, S., Link, S., Thanisch, K., Mulholland, C., et al. (2022). Spatial organization of transcribed eukaryotic genes. Nat. Cell Biol. *24*, 327–339. https://doi.org/10.1038/s41556-022-00847-6.

Lengronne, A., Katou, Y., Mori, S., Yokobayashi, S., Kelly, G.P., Itoh, T., Watanabe, Y., Shirahige, K., and Uhlmann, F. (2004). Cohesin relocation from sites of chromosomal loading to places of convergent transcription. Nature *430*, 573–578.

Lieberman-Aiden, E., van Berkum, N.L., Williams, L., Imakaev, M., Ragoczy, T., Telling, A., Amit, I., Lajoie, B.R., Sabo, P.J., Dorschner, M.O., et al. (2009). Comprehensive mapping of long-range interactions reveals folding principles of the human genome. Science *326*, 289–293.

Li, H. (2013). Aligning sequence reads, clone sequences and assembly contigs with BWA-MEM. Preprint at arXiv. http://arxiv.org/abs/1303.3997.

Love, M.I., Huber, W., and Anders, S. (2014). Moderated estimation of fold change and dispersion for RNA-seq data with DESeq2. Genome Biol. *15*, 550.

Lu, F., and Lionnet, T. (2021). Transcription factor dynamics. Cold Spring Harbor Perspect. Biol. *13*, a040949. https://doi.org/10.1101/cshperspect.a040949.

Marcel, S.S., Quimby, A.L., Noel, M.P., Jaimes, O.C., Mehrab-Mohseni, M., Ashur, S.A., Velasco, B., Tsuruta, J.K., Kasoji, S.K., Santos, C.M., and Dayton, P.A. (2021). Genome-wide cancer-specific chromatin accessibility patterns derived from archival processed xenograft tumors. Genome Res. *31*, 2327–2339. https://doi.org/10.1101/gr.275219.121.

Monahan, K., Horta, A., and Lomvardas, S. (2019). LHX2- and LDB1-mediated trans interactions regulate olfactory receptor choice. Nature *565*, 448–453.

Mumbach, M.R., Rubin, A.J., Flynn, R.A., Dai, C., Khavari, P.A., Greenleaf, W.J., and Chang, H.Y. (2016). HiChIP: efficient and sensitive analysis of protein-directed genome architecture. Nat. Methods *13*, 919–922.

Olan, I., Parry, A.J., Schoenfelder, S., Narita, M., Ito, Y., Chan, A.S.L., Slater, G.S.C., Bihary, D., Bando, M., Shirahige, K., et al. (2020). Transcription-dependent cohesin repositioning rewires chromatin loops in cellular senescence. Nat. Commun. *11*, 6049.

Olshansky, M. (2021). EigenVector, EigenVector GitHub. https://github.com/moshe-olshansky/EigenVector.

Patro, R., Duggal, G., Love, M.I., Irizarry, R.A., and Kingsford, C. (2017). Salmon provides fast and bias-aware quantification of transcript expression. Nat. Methods *14*, 417–419.

Phanstiel, D.H., Van Bortle, K., Spacek, D., Hess, G.T., Shamim, M.S., Machol, I., Love, M.I., Aiden, E.L., Bassik, M.C., and Snyder, M.P. (2017). Static and dynamic DNA loops form AP-1-bound activation hubs during macrophage development. Mol. Cell *67*, 1037–1048.e6.

Picard, no date. https://broadinstitute.github.io/picard/.

Pradhan, B., Barth, R., Kim, E., Davidson, I.F., Bauer, B., van Laar, T., Yang, W., Ryu, J.K., van der Torre, J., Peters, J.M., and Dekker, C. (2021). SMC complexes can traverse physical roadblocks bigger than their ring size. Preprint at bioRxiv. https://doi.org/10.1101/2021.07.15.452501.

Quinlan, A.R., and Hall, I.M. (2010). BEDTools: a flexible suite of utilities for comparing genomic features. Bioinformatics *26*, 841–842.

Ramírez, F., Ryan, D.P., Grüning, B., Bhardwaj, V., Kilpert, F., Richter, A.S., Heyne, S., Dündar, F., and Manke, T. (2016). deepTools2: a next generation web server for deep-sequencing data analysis. Nucleic Acids Res. *44*, W160–W165.

Rao, S.S.P., Huntley, M.H., Durand, N.C., Stamenova, E.K., Bochkov, I.D., Robinson, J.T., Sanborn, A.L., Machol, I., Omer, A.D., Lander, E.S., and Aiden, E.L. (2014). A 3D map of the human genome at kilobase resolution reveals principles of chromatin looping. Cell *159*, 1665–1680.

Rao, S.S.P., Huang, S.C., Glenn St Hilaire, B., Engreitz, J.M., Perez, E.M., Kieffer-Kwon, K.R., Sanborn, A.L., Johnstone, S.E., Bascom, G.D., Bochkov, I.D., et al. (2017). Cohesin loss eliminates all loop domains. Cell *171*, 305–320.e24.

R Core Team (2022). R: A Language and Environment for Statistical Computing (R Foundation for Statistical Computing). https://www.R-project.org.

Rosencrance, C.D., Ammouri, H.N., Yu, Q., Ge, T., Rendleman, E.J., Marshall, S.A., and Eagen, K.P. (2020). Chromatin hyperacetylation impacts chromosome folding by forming a nuclear subcompartment. Mol. Cell *78*, 112–126.e12.

Rowley, M.J., Poulet, A., Nichols, M.H., Bixler, B.J., Sanborn, A.L., Brouhard, E.A., Hermetz, K., Linsenbaum, H., Csankovszki, G., Lieberman Aiden, E., and Corces, V.G. (2020). Analysis of Hi-C data using SIP effectively identifies loops in organisms from C. elegans to mammals. Genome Res. *30*, 447–458.

Rowley, M.J., and Corces, V.G. (2018). Organizational principles of 3D genome architecture. Nat. Rev. Genet. *19*, 789–800.

Sanborn, A.L., Rao, S.S.P., Huang, S.C., Durand, N.C., Huntley, M.H., Jewett, A.I., Bochkov, I.D., Chinnappan, D., Cutkosky, A., Li, J., et al. (2015). Chromatin extrusion explains key features of loop and domain formation in wild-type and engineered genomes. Proc. Natl. Acad. Sci. USA *112*, E6456–E6465.

Schoenfelder, S., and Fraser, P. (2019). Long-range enhancer–promoter contacts in gene expression control. Nat. Rev. Genet. *20*, 437–455. https://doi.org/10.1038/s41576-019-0128-0.

Schwarzer, W., Abdennur, N., Goloborodko, A., Pekowska, A., Fudenberg, G., Loe-Mie, Y., Fonseca, N.A., Huber, W., Haering, C.H., Mirny, L., and Spitz, F. (2017). Two independent modes of chromatin organization revealed by cohesin removal. Nature *551*, 51–56.

Simonis, M., Klous, P., Splinter, E., Moshkin, Y., Willemsen, R., de Wit, E., van Steensel, B., and de Laat, W. (2006). Nuclear organization of active and inactive chromatin domains uncovered by chromosome conformation capture–on-chip (4C). Nat. Genet. *38*, 1348–1354.

Soneson, C., Love, M.I., and Robinson, M.D. (2015). Differential analyses for RNA-seq: transcript-level estimates improve gene-level inferences. F1000Res. *4*, 1521.

Spielmann, M., Lupiáñez, D.G., and Mundlos, S. (2018). Structural variation in the 3D genome. Nat. Rev. Genet. *19*, 453–467.

Stigler, J., Çamdere, G.Ö., Koshland, D.E., and Greene, E.C. (2016). Single-molecule imaging reveals a collapsed conformational state for DNA-bound cohesin. Cell Rep. *15*, 988–998. https://doi.org/10.1016/j.celrep.2016.04.003.

Stik, G., Vidal, E., Barrero, M., Cuartero, S., Vila-Casadesús, M., Mendieta-Esteban, J., Tian, T.V., Choi, J., Berenguer, C., Abad, A., et al. (2020). CTCF is dispensable for immune cell transdifferentiation but facilitates an acute inflammatory response. Nat. Genet. *52*, 655–661.

Vian, L., Pękowska, A., Rao, S.S.P., Kieffer-Kwon, K.R., Jung, S., Baranello, L., Huang, S.C., El Khattabi, L., Dose, M., Pruett, N., et al. (2018). The energetics and physiological impact of cohesin extrusion. Cell *175*, 292–294.

Vilarrasa-Blasi, R., Soler-Vila, P., Verdaguer-Dot, N., Russiñol, N., Di Stefano, M., Chapaprieta, V., Clot, G., Farabella, I., Cuscó, P., Kulis, M., et al. (2021). Dynamics of genome architecture and chromatin function during human B cell differentiation and neoplastic transformation. Nat. Commun. *12*, 651.

Winick-Ng, W., Kukalev, A., Harabula, I., Zea-Redondo, L., Szabó, D., Meijer, M., Serebreni, L., Zhang, Y., Bianco, S., Chiariello, A.M., et al. (2021). Cell-type specialization is encoded by specific chromatin topologies. Nature *599*, 684–691.

Xiao, J.Y., Hafner, A., and Boettiger, A.N. (2021). How subtle changes in 3D structure can create large changes in transcription. Elife *10*, e64320. https://doi.org/10.7554/eLife.64320.

Yang, J., McGovern, A., Martin, P., Duffus, K., Ge, X., Zarrineh, P., Morris, A.P., Adamson, A., Fraser, P., Rattray, M., and Eyre, S. (2020). Analysis of chromatin organization and gene expression in T cells identifies functional genes for rheumatoid arthritis. Nat. Commun. *11*, 4402.

Zhang, H., Emerson, D.J., Gilgenast, T.G., Titus, K.R., Lan, Y., Huang, P., Zhang, D., Wang, H., Keller, C.A., Giardine, B., et al. (2019a). Chromatin structure dynamics during the mitosis-to-G1 phase transition. Nature *576*, 158–162.

Zhang, S., Übelmesser, N., Barbieri, M., and Papantonis, A. (2022). Enhancer-promoter contact formation requires RNAPII and antagonizes loop extrusion. Preprint at bioRxiv. https://doi.org/10.1101/2022.07.04.498738.

Zhang, Y., Liu, T., Meyer, C.A., Eeckhoute, J., Johnson, D.S., Bernstein, B.E., Nusbaum, C., Myers, R.M., Brown, M., Li, W., and Liu, X.S. (2008). Model-based analysis of ChIP-seq (MACS). Genome Biol. *9*, R137.

Zhang, Y., Li, T., Preissl, S., Amaral, M.L., Grinstein, J.D., Farah, E.N., Destici, E., Qiu, Y., Hu, R., Lee, A.Y., et al. (2019b). Transcriptionally active HERV-H retrotransposons demarcate topologically associating domains in human pluripotent stem cells. Nat. Genet. *51*, 1380–1388.

Zheng, H., and Xie, W. (2019). The role of 3D genome organization in development and cell differentiation. Nat. Rev. Mol. Cell Biol. *20*, 535–550.

Zhu, A., Ibrahim, J.G., and Love, M.I. (2019). Heavy-tailed prior distributions for sequence count data: removing the noise and preserving large differences. Bioinformatics *35*, 2084–2092.

## STAR★METHODS

### KEY RESOURCES TABLE

| REAGENT or RESOURCE | SOURCE | IDENTIFIER |
|---|---|---|
| Antibodies | | |
| Anti-Histone H3 (acetyl K27) antibody - ChIP Grade, rabbit | AbCam | Cat# ab4729; RRID: AB_2118291 |
| Chemicals, peptides, and recombinant proteins | | |
| Corning cellgro RPMI-1640 medium with L-Glutamine | Fisher Scientific | Cat# MT10040CV |
| Fetal bovine serum | Fisher Scientific | Cat# 26-140-079 |
| Penicillin-Streptomycin | Fisher Scientific | Cat# 15-140-122 |
| 12-O-tetradecanoylphorbol-l3-acetate (PMA) | Sigma-Aldrich | Cat# P1585-1MG |
| Lipopolysaccharides (LPS) from Escherichia coli | Sigma-Aldrich | Cat# L2630-10MG |
| Recombinant human interferon type gamma (IFNγ) | Peprotech | Cat# 300-02 |
| Formaldehyde, 37% w/v | Fisher Scientific | Cat# F79-500 |
| UltraPure Glycine | Invitrogen | Cat# 15527013 |
| 1.0 M HEPES, pH 8 | Fisher Scientific | Cat# AAJ63578AK |
| 5 M NaCl | Sigma-Aldrich | Cat# 71386-1L |
| 0.5 M EDTA | VWR | Cat# 351-027-721EA |
| glycerol | VWR | 97062-832 |
| 10% NP-40 | Fisher Scientific | Cat# PI85124 |
| 10% Triton X-100 | Signa-Aldrich | Cat# 93443-100ML |
| 1 M Tris-HCl, pH 8.0 | Fisher Scientific | Cat# 15-567-025 |
| 1 M Tris-HCl, pH 7.5 | Fisher Scientific | Cat# 15-567-027 |
| 0.5 M EGTA | Fisher Scientific | Cat# NC0300614 |
| 10% SDS | Fisher Scientific | Cat# 15-553-027 |
| 3 M Sodium acetate | Sigma-Aldrich | Cat# S7899-100ML |
| Tween 20 | Sigma-Aldrich | Cat# P9416-100ML |
| IGEPAL CA-630 | Sigmal-Aldrich | Cat# I8896-50ML |
| Protease inhibitor cocktail | Sigma-Aldrich | Cat# P8340-5ML |
| Nanodroplets (C18) | Triangle Biotechnology, Inc (Marcel et al., 2021) | FF101-5000 |
| Proteinase K | VWR | Cat# 97062-670 |
| RNase A | Fisher Scientific | Cat# FEREN0531 |
| Dulbeccos PBS (1×) w/o $Ca^{2+}$ or Mg2+ | Sigma-Aldrich | Cat# PBS2541 |
| Pure ethanol (200 proof) | Fisher Scientific | Cat# 07-678-003 |
| 10X NEBuffer 2 | NEB | Cat# B7002S |
| MboI restriction enzyme | NEB | Cat# R0147S |
| Biotin-14-dATP | Life Technologies | Cat# 19524-016 |
| DNA Polymerase I, Large Klenow Fragment | NEB | Cat# M0210L |
| 10X NEB T4 DNA ligase buffer | NEB | Cat# B0202S |
| BSA (20 mg/mL) | NEB | Cat# B9000S |
| T4 DNA ligase (2,000,000 U/mL) | NEB | Cat# M0202T |
| Proteinase K | NEB | Cat# P8107S |
| Agencourt AMPure XP beads | Beckman Coulter | Cat# A63881 |
| Dynabeads MyOne Streptavidin T1 beads | ThermoFisher | Cat# 65601 |
| 100 mM dNTP Solution Set | NEB | Cat# N0446S |
| NEB T4 Polynucleotide kinase (PNK) | NEB | Cat# M0201S |

(*Continued on next page*)

*Continued*

| REAGENT or RESOURCE | SOURCE | IDENTIFIER |
|---|---|---|
| NEB T4 DNA polymerase I | NEB | Cat# M0203S |
| NEB Klenow Fragment (3'→5' exo-) | NEB | Cat# M0212L |
| 5X Quick Ligation Reaction Buffer | NEB | Cat# B6058S |
| NEB DNA Quick Ligase | NEB | Cat# M2200S |
| **Critical commercial assays** | | |
| RNeasy Mini Kit with DNase I treatment | Qiagen | Cat# 74104 |
| Tapestation RNA ScreeTape | Agilent Technologies | Cat# 5067-5576 |
| Qubit RNA High Sensitivity Assay | Fisher Scientific | Cat# Q32852 |
| NEB rRNA Depletion Kit (Human/Mouse/Rat) with RNA Sample Purification Beads | NEB | Cat# E6350L |
| Qubit dsDNA High Sensitivity Assay | Fisher Scientific | Cat# Q32854 |
| Tapestation HS D1000 ScreenTape | Agilent Technologies | Cat# 5067-5584 |
| Illumina NextSeq 500 High Output Kit | Illumina | Cat# 20024907 |
| Zymo ChIP DNA Clean & Concentrator Kit | Zymo Research | Cat# D5205 |
| Qubit dsDNA Broad Range Assay | Fisher Scientific | Cat# Q32850 |
| ChIP-IT High Sensitivity Kit | Active Motif | Cat# 53040 |
| NEBNext DNA Ultra II DNA Library Prep w/Sample Purifcation Beads | NEB | Cat# E7103S |
| NEBNext Multiplex Oligos for Illumina (Index Primers Set 1) | NEB | Cat# E7335S |
| TruSeq Nano DNA LT Library Preparation Kit - Set A | Illumina | Cat# FC-121-4001 |
| Nextera®DNA Library Preparation Kit (24 samples) | Illumina | Cat# FC-121-1030 |
| Nextera XT Index Kit (24 indexes, 96 samples) | Illumina | Cat# FC-131-1001 |
| KAPA Library Quantification Kit | KAPA Biosystems | Cat# 4854 |
| **Deposited data** | | |
| *in situ* Hi-C in THP-1-derived macrophages activated by LPS/IFNg (raw) | SRA | SRA: PRJNA831239 |
| *in situ* Hi-C in THP-1-derived macrophages activated by LPS/IFNg (processed) | GEO | GEO: GSE201353 |
| RNA-Seq in THP-1-derived macrophages activated by LPS/IFNg (raw) | SRA | SRA: PRJNA830916 |
| RNA-Seq in THP-1-derived macrophages activated by LPS/IFNg (processed) | GEO | GEO: GSE201354 |
| ATAC-Seq in THP-1-derived macrophages activated by LPS/IFNg (raw) | SRA | SRA: PRJNA830918 |
| ATAC-Seq in THP-1-derived macrophages activated by LPS/IFNg (processed) | GEO | GEO: GSE201351 |
| H3K27ac ChIP-Seq in THP-1-derived macrophages activated by LPS/IFNg (raw) | SRA | SRA: PRJNA830917 |
| H3K27ac ChIP-Seq in THP-1-derived macrophages activated by LPS/IFNg (processed) | GEO | GEO: GSE201352 |
| **Experimental models: Cell lines** | | |
| *H. sapiens* THP-1 monocyte cell line | ATCC | Cat# TIB-202; RRID: CVCL_0006 |
| **Software and algorithms** | | |
| Trim Galore! (version 0.4.3) | Babraham Bioinformatics, 2015 | http://www.bioinformatics.babraham.ac.uk/projects/trim_galore/ |
| BWA mem (version 0.7.17) | Li (2013) | http://bio-bwa.sourceforge.net/ |
| PicardTools (version 2.10.3) | Broad Institute, 2019 | https://broadinstitute.github.io/picard/ |
| Samtools (version 1.9) | Danecek et al. (2021) | http://www.htslib.org/ |
| MACS2 (version 2.1.1.20160309) | Zhang et al. (2008) | https://github.com/macs3-project/MACS |

(*Continued on next page*)

*Continued*

| REAGENT or RESOURCE | SOURCE | IDENTIFIER |
|---|---|---|
| bedtools (version 2.28) | Quinlan and Hall (2010) | https://bedtools.readthedocs.io/en/latest/ |
| FastQC (version 0.11.5) | Babraham Bioinformatics, 2010 | https://www.bioinformatics.babraham.ac.uk/projects/fastqc/ |
| MultiQC (version 1.5) | Ewels et al. (2016) | https://multiqc.info/ |
| R (version 3.3.1) | R Core Team (2022) | https://www.R-project.org |
| DESeq2 (version 1.33.5) | Love et al. (2014) | https://github.com/mikelove/DESeq2 |
| Juicer (version 1.5.6) | Rao et al. (2014) | https://github.com/aidenlab/juicer |
| SIP (version 1.6.1) | Rowley et al. (2020) | https://github.com/PouletAxel/SIP |
| DBScan (version (1.1.8) | Hahsler et al. (2019) | https://CRAN.R-project.org/package=dbscan |
| strawr (version 0.0.9) | Durand et al. (2016) | https://github.com/aidenlab/straw/tree/master/R |
| tximport (version 1.2.0) | Soneson et al. (2015) | https://github.com/mikelove/tximport |
| Salmon (version 1.4.0) | Patro et al. (2017) | https://combine-lab.github.io/salmon/ |
| HISAT2 (version 2.1.0) | Kim et al. (2019) | http://daehwankimlab.github.io/hisat2/ |
| deeptools (version 3.0.1) | Ramirez et al. (2016) | https://deeptools.readthedocs.io/en/develop/ |
| nullranges (version 1.2.0) | Davis et al. (2022) | https://nullranges.github.io/nullranges/index.html |
| CTCF (version 0.99.4) | Dozmorov et al., 2022 | https://github.com/mdozmorov/CTCF |

## RESOURCE AVAILABILITY

### Lead contact

Further information and requests for resources and reagents should be directed to and will be fulfilled by the lead contact Douglas Phanstiel (douglas_phanstiel@med.unc.edu).

### Materials availability

This study did not generate new unique reagents.

### Data and code availability

- Processed data for Hi-C, RNA-seq, ATAC-seq, and ChIP-seq data are publicly available on GEO: SuperSeries GSE201376. Raw data for each are publicly available on SRA. Individual accession numbers are listed in the key resources table.
- This paper does not report original code.
- Any additional information required to reanalyze the data reported in this paper is available from the lead contact upon request.

## EXPERIMENTAL MODEL AND SUBJECT DETAILS

### Cell lines

Human male THP-1 monocytes (RIID CVCL_0006, ATCC TIB-202) were grown and maintained in RPMI media with 10% fetal bovine serum (FBS) and 1% penicillin-streptomycin (PS). Cells were routinely checked for mycoplasma using Genetic Cell Line Testing and confirmed negative. Cell lines were also authenticated using STR analysis via the UNC Vironomics Core.

## METHOD DETAILS

### Macrophage differentiation and activation

For differentiation into macrophages, THP-1 monocytes were transferred to 6-well plates (RNA-seq, ATAC-seq) or T-175 flasks (Hi-C, ChIP-seq) at a density of $2 \times 10^5$ cells/mL and treated with 25 nM PMA for 24 h, over which time the cells become adherent. The media was then aspirated off, the flasks were washed gently with RPMI, and then fresh RPMI (10% FBS, 1% PS) and rested for 72 h.

The resting macrophages were then treated with a combination of 10 ng/mL lipopolysaccharide (LPS) and 20 ng/mL interferon gamma ($IFN_\gamma$) in fresh RPMI (10% FBS, 1% PS). Cells were harvested without treatment, or 0.5, 1, 1.5, 2, 4, 6, or 24 h after LPS and $IFN_\gamma$ treatment.

During each treatment, extra 0- and 2-h samples were prepared simultaneously for RNA extraction, and qPCR was used to measure the regulation of FOS, IL1B and IL6 to confirm consistent treatment response.

For all library preparations, the differentiation and activation treatment was performed from freshly thawed THP-1 cells on two separate occasions, to achieve the closest approximation to two biological replicates using cultured cell types.

### Crosslinking

For ChIP-seq and Hi-C, cells were grown in T-175 flasks, each containing $20 \times 10^6$ cells at a density of $2 \times 10^5$ cells/mL. Cells were crosslinked using 1% formaldehyde in RPMI for 10 min with gentle shaking. Crosslinking was then quenched with 10% 2.0 M cold glycine for 5 min. The media was then removed and cells were scraped into cold PBS. Each flask was divided into 4 tubes of approximately $5 \times 10^6$ cells each. Cells were spun down at 526 G for 5 m, resuspended in PBS and respun to wash away residual formaldehyde. Cells were then frozen in liquid nitrogen and stored at −80 for library preparation.

### RNA-seq library preparation

RNA was extracted using the QIAGEN RNeasy Mini kit with DNase I treatment. RNA integrity numbers were confirmed using a Tapestation RNA screentape to be above 9.8, and a Qubit High Sensitivity assay was used to determine RNA concentration.

Ribosomal RNA was removed using the NEB rRNA Depletion Kit (Human/Mouse/Rat) using 500 ng of RNA as input. Following depletion, RNA-seq libraries were prepared using the NEB Ultra II Directional RNA Library Prep Kit for Illumina, and NEBNext Multiplex Oligos for Illumina. Library concentration and fragment size was determined using Qubit (dsDNA HS assay) and Tapestation (D1000 screentape). Libraries from each timepoint were pooled to a final DNA concentration of 15 nM, and 75-bp paired-end reads were sequenced on an Illumina NextSeq 500 using a High Output Kit.

### ChIP-seq library preparation

Four frozen cell pellets ($5 \times 10^6$ cells each) were used for each timepoint. Pellets were first rinsed in 10 mL rinse buffer 1 (50 mM HEPES pH 8, 140 mM NaCl, 1 mM EDTA, 10% glycerol, 0.5% NP-40, Triton-X), incubated on ice for 10 min, and then spun down at 2,400 G at 4°C for 5 min. Supernatant was removed and the pellets were rinsed again in rinse buffer 2 (10 mM Tris pH 8, 1 mM EDTA, 0.5 mM EGTA, 200 mM NaCl), and spun at the same settings. Supernatant was removed, and 5 mL of shearing buffer (10 mM Tris pH 8, 2% Triton-X, 1% SDS, 100 mM NaCl, 1 mM EDTA) was added to the tubes to wash out the rinse buffer. The samples were centrifuged at 2,400G at 4°C for 3 min, the shearing buffer was removed and this step was repeated. The cell pellets were then resuspended in 88 uL of shearing buffer, 2 uL of protease inhibitor cocktail (PIC), and 10 uL of nanodroplets (Triangle Biotechnology, Inc.) per 10 million cells (Kasoji et al., 2015; Marcel et al., 2021). Samples were aliquoted into 100 uL tubes and sheared using a Covaris E110 (intensity 6, 210 s). Cells were spun down at max speed for 2 min and the supernatant was retained.

In order to determine the concentration of chromatin, 10 uL was removed (while the rest of the sample was stored at −80°C), and crosslinking was reversed by adding 5 uL of 5 M NaCl, 125 uL of TE buffer (10 mM Tris pH 8, 1 mM EDTA) and 125 uL of elution buffer (1 M Tris pH 8, 10 mM EDTA, 1% SDS), vortexed, and incubated overnight at 65°C. Samples were spun down and added 7.5 uL of proteinase K and 3 uL of RNase A. DNA was extracted using the Zymo ChIP DNA Clean & Concentrator Kit, quantified using Qubit (dsDNA broad-range (BR) assay), and run on a gel to ensure fragment sizes of 100–300 bp and concentrations high enough to continue with library prep.

Immunoprecipitation of the remaining volume from each sheared sample was completed using the Active Motif ChIP-IT High Sensitivity kit, using 2.8 ug of chromatin from each timepoint (as determined by the lowest yield samples), and 4 ug of anti-H3K27ac antibody (AbCam ab4729). Following overnight antibody incubation and washing steps, crosslinking was reversed by adding 100 uL of elution buffer (described previously) and 4 uL of 5 M NaCl to 100 uL of the IP reactions, vortexing, and then incubating overnight at 65°C. DNA was purified using the Zymo ChIP DNA Clean & Concentrator kit, and quantified using Qubit (dsDNA high-sensitivity (HS) assay), as before.

Following the final dilution, libraries were prepared using the NEB Ultra II DNA Library Prep Kit with NEBNext Multiplex Oligos for Illumina with 0.88 ng of DNA as input. Libraries were analyzed using Qubit (dsDNA HS assay) and Tapestation (D1000 screentape) and pooled to a final concentration of 12 nM, and then 75-bp paired-end reads were sequenced on an Illumina NextSeq 500 using a High Output Kit.

### *In situ* Hi-C library preparation

Three treatments (biological replicates) were conducted, and one or two frozen cell pellets ($5 \times 10^6$ cells each) were used to generate separate libraries as technical replicates (1 technical replicate for first biological replicate; 2 technical replicates for second and third biological replicates). Libraries were prepared using the *in situ* Hi-C protocol as described in Rao et al. (2014) (Rao et al., 2014). In brief, crosslinked cells were lysed on ice, nuclei were isolated, and chromatin was digested overnight with the MboI restriction enzyme. Chromatin ends were biotinylated, proximity ligated, and crosslinking was reversed. Samples were sheared on a Covaris LE 220 (DF 25, PIP 500, 200 cycles/burst, 90 s), quantified using Qubit (dsDNA High Sensitivity (HS) assay), and a small sample was run on an agarose gel to ensure proper fragmentation. DNA sized 300–500 bp was selected for using AMPure XP beads, and then eluted. Biotinylated chromatin was then pulled down using streptavidin beads. Following removal of biotin from unligated ends and repair of sheared DNA ends, unique Illumina TruSeq Nano (Set A) indices were ligated onto the samples. Libraries were

amplified off of streptavidin beads using 7–10 PCR cycles based on post-size selection concentrations, quantified again using a Qubit (dsDNA HS assay), and fragment length was determined using Tapestation (D1000 screentape). Libraries were pooled to 10 nM. Paired-end 150-bp reads were sequenced on one or two lanes of an Illumina NovaSeq S4.

### ATAC-seq library preparation

ATAC-seq libraries were prepared using the Omni ATAC-seq protocol as described in Corces et al. (2017). Adherent macrophages were washed once with PBS and lifted off of the plate with EDTA for 5 min. EDTA was quenched with RPMI, and library preparation was performed on 50,000 cells. 3.75 μL of Illumina Nextera XT indices were used in PCR and qPCR.

After performing the initial 5 cycles of PCR, 5% of the PCR reaction was used in qPCR to determine how many additional cycles were required. 4–7 cycles were determined to be sufficient for the final amplification. A 2-sided bead cleanup with AMPure XP beads was performed (0.5X, then 1.3X). Libraries were quantified using Qubit (dsDNA HS Assay) and the KAPA Library Quantification kit. Libraries from each timepoint were pooled to a concentration of 8 nM or 10 nM for each biological replicate, and 75-bp paired-end reads were sequenced on an Illumina NextSeq 500 using a High Output Kit.

## QUANTIFICATION AND STATISTICAL ANALYSIS

### RNA-seq processing and gene quantification

Adaptors and low-quality reads were trimmed from paired-end reads using Trim Galore! (version 0.4.3; Babraham Bioinformatics, 2015). Salmon (version 1.4.0; Patro et al., 2017) was used in quant mode to quantify reads to hg19 transcripts from GENCODE (version 19). For signal tracks, reads were aligned using HISAT2 (version 2.1.0; Kim et al., 2019), indexed and replicates were merged with samtools (version 1.9; Danecek et al., 2021), and converted to bigwigs using deeptools (version 3.0.1; Ramírez et al., 2016). Reads were summarized to a gene level using tximport (R version 3.3.1, tximport version 1.2.0; R Core Team, 2022; Soneson et al., 2015), which was then used as input for differential analysis in DESeq2 (version 1.33.5; Love et al., 2014). FastQC and MultiQC were used to assess library quality metrics (version 0.11.5; version 1.5; Babraham Bioinformatics, 2010; Ewels et al., 2016).

### Inferred transcription score (ITS) calculations

Inferred transcription scores (ITS) were calculated in order to estimate the degree of transcription occurring throughout gene bodies, including introns, as extrapolated from the mature mRNA TPM levels. Gene-level TPM as quantified by Salmon and summarized by txImport (see RNA-seq processing methods). The genome was binned into 10-kb or 50-kb regions using bedtools makewindows (version 2.28), and then overlapped with gene bodies (Quinlan and Hall, 2010). Gene TPM values were applied to each overlapping bin, adjusted based on the percentage of bin overlap. For example, a gene of TPM 50 with a TSS at position 100,000 bp and a TTS at position 115,000 bp would contribute an ITS of 50 to the bin of 100,000–110,000, and an ITS of 25 to the bin of 110,000–120,000. In bins with multiple genes, ITS scores were generated by summing the TPM contribution from each gene.

### ATAC- and ChIP-seq processing and peak calling

Adaptors and low-quality reads were trimmed from paired-end reads using Trim Galore! (version 0.4.3; Babraham Bioinformatics, 2015). Reads were aligned using BWA mem (version 0.7.17; Li, 2013) and sorted using Samtools (version 1.9; Danecek et al., 2021). Duplicates were removed with PicardTools (version 2.10.3; Picard, no date) and for ATAC-seq libraries, mitochondrial reads were removed using Samtools idxstats. Samtools was also used to merge replicates for each timepoint, and index BAM files. Peaks were called from the merged alignments using MACS2 with the following settings: -f BAM -q 0.01 -g hs –nomodel –extsize 200 –keep-dup all -B –SPMR (version 2.1.1.20160309; Zhang et al., 2008). ChIP-seq peaks used the MACS2 setting –shift 0, while ATAC-seq peaks used –shift 100. Peaks from all timepoints were then merged using bedtools (version 2.28; Quinlan and Hall, 2010), generating 118,344 ChIP-seq and 193,853 ATAC-seq peaks in total. For each replicate BAM file, ChIP-seq counts were extracted from ATAC-seq peak locations using bedtools multicov. Bedtools intersect was used to subset for ATAC-seq peaks that overlapped H3K27ac ChIP-seq peaks, and these 89,503 peaks were considered putative regulatory regions. Raw counts at these enhancers (8 timepoints, 2 replicates each) were used as input for differential analysis with DESeq2 (version 1.33.5; Love et al., 2014). Signal tracks were made from alignments using deeptools (version 3.0.1; Ramírez et al., 2016).

### Enhancer and promoter definitions

Gene promoters were identified as regions 2,000 base pairs upstream and 200 base pairs downstream of gene transcriptional start sites (TSS). Promoter H3K27ac signal was calculated based on any overlapping H3K27ac and ATAC-seq peaks within promoter regions using bedtools intersect (version 2.28; Quinlan and Hall, 2010). Enhancers were identified as overlapping H3K27ac and ATAC-seq peaks that did not overlap with defined promoter regions.

### Predicted CTCF binding sites

Directional predicted CTCF binding sites for hg19 were obtained from AnnotationHub ID AH95565 using the "CTCF" R package (Dozmorov et al., 2022). The specific track used here features data from UCSC Jaspar, and represents the hg19 coordinates of binding motif MA0139.1 as detected by FIMO.

### Hi-C processing, loop and compartment calling

Hi-C data were processed using the Juicer pipeline as initially described in Rao et al. (version 1.5.6; Rao et al., 2014). Hi-C maps were made at 5- and 10-kb resolution for each technical replicate (8 timepoints, each with 5 technical replicates across 3 biological replicates), as well as for each timepoint (all replicates combined). Additionally, a "Mega" map from all timepoints was made, also using Juicer.

Loops were identified at 5-kb using SIP (version 1.6.1; Rowley et al., 2020). Loops were called from the individual timepoint maps using the settings "-g 2 -t 2000 -fdr 0.05", and from the Mega map with the settings "-g 1 -t 2000 -fdr 0.05". The loops were then extrapolated to 10-kb, concatenated, and merged in R using DBScan (version 1.1.8; Hahsler et al., 2019) with an epsilon of 20 kb (manhattan distance), keeping the mean of modes for coordinates, resulting in 42,690 total loops. The counts for these loops were then extracted from the Hi-C files of each technical replicate (un-normalized, 10-kb resolution) using strawr (version 0.0.9; Durand et al., 2016). These raw counts (8 timepoints, 3 biological replicates each, two with 2 technical replicates and one with 1 technical replicate each) were used as input for differential analysis with DESeq2 (Love et al., 2014).

Compartments were called for Hi-C biological replicates 2 and 3 using the EigenVector script at a 50-kb resolution (Olshansky, 2021). Biological replicate 1 was not used for this analysis due to its decreased sequencing depth and the method of differential compartment calling (see "differential compartment and ITS bin analysis" section below). The A compartment was determined based on gene content overlap on a per-chromsome basis.

### Differential gene and peak analysis

DESeq2 was used for differential analysis of genes, loops, and peaks (Love et al., 2014). Each analysis used a likelihood ratio test (LRT), with a full design of "~bioRep + time" and a reduced design of "~bioRep". Posterior log-2 fold changes (LFC) were estimated using apeglm (Zhu et al., 2019). Significant results were determined based on an absolute LFC greater than 1 and an adjusted p value below 0.01.

Raw counts were converted into Z-scores by first conducting a variance-stabilizing transformation across all features, and then centering and scaling the data in each feature based on standard deviations from the mean. Genes were categorized into up- and downregulated based on the signage of their Z-score at 0 h of LPS/IFNg treatment, and then sorted based on their timepoint of maximum Z-score.

### Differential loop analysis and clustering

DESeq2 was also used for differential analysis of loops (Love et al., 2014). Differential analysis used a likelihood ratio test (LRT), with a full design of "~techRep + bioRep + time", and a reduced design of "~techRep + bioRep". Significant results were determined based on an absolute LFC greater than 0.585 (fold-change of ±1.5) and an adjusted p value below 0.05.

Raw counts were converted into Z-scores by first conducting a variance-stabilizing transformation across all features, and then centering and scaling the data in each feature based on standard deviations from the mean. These Z-scores were then used to cluster loops using k-means clustering (k = 4). For the survey of loop contacts at the GBP locus, log2 observed/expected KR-normalized counts were extracted using strawr.

#### *Differential compartment and ITS bin analysis and clustering*

Compartment eigenvectors (EV) and ITS values were both binned at 50-kb for comparison and overlap. Differential EV and ITS bins were identified based on an average raw difference of 0.5 (EV) or a fold-change of 2 (ITS) between any timepoint and 0 h. False-positive rates of 13.4% for EV and 10.7% for ITS were calculated by finding the number of bins with differences beyond these thresholds between biological replicates (regarded as false positives) out of the total number of bins passing the threshold. ITS bins were further subset for bins containing a score of 5 or higher in any biological replicate. A total of 5,611 differential EV bins were found, and a 8,068 differential ITS bins were found, with 930 bins that were differential for both.

Differential compartment and ITS bins were then categorized according to their timing and direction of change. First, z-scores were calculated for each bin at each timepoint by meaning the eigenvector or ITS values between replicates, then centering and scaling the data. The overall direction (up or down) of each differential bin was determined based on the sign of their initial z-score. Based on these categorizations, 81.2% of overlapping differential bins have EV and ITS that changed in the same direction. The increasing and decreasing bins were then further categorized by the timepoint of minimum or maximum z-score (30 min–24 h), as for differential gene categorization.

### Matched enhancer-promoter sets

Covariate-matched subset selection among non-looped enhancer-promoter pairs was performed using the *matchRanges* function from the *nullranges* package (Davis et al., 2022). Enhancer-promoter pair distance or total contact frequency were used as covariates. Total contact frequency was calculated from KR normalized counts from the combined Mega map, effectively a sum of contacts across all timepoints and replicates. Matching was done with the stratified matching method without replacement. Enhancer strength, defined by the sum of H3K27ac variance-stabilized counts across all timepoints and replicates, was compared between the looped and matched non-looped sets.